University of Alberta

Fiber Optic Based Tunable Diode Laser Gas Detector

by

Gerald R. Beaudoin

©

A thesis submitted to the Faculty of Graduate Studies and Research in partial fulfillment of the requirements of the degree of Master of Science.

Department of Electrical and Computer Engineering

Edmonton, Alberta
Spring 2000

National Library of Canada
Acquisitions and Bibliographic Services
395 Wellington Street
Ottawa ON K1A 0N4
Canada

Bibliothèque nationale du Canada
Acquisitions et services bibliographiques
395, rue Wellington
Ottawa ON K1A 0N4
Canada

Your file Votre référence

Our file Notre référence

The author has granted a non-exclusive licence allowing the National Library of Canada to reproduce, loan, distribute or sell copies of this thesis in microform, paper or electronic formats.

L'auteur a accordé une licence non exclusive permettant à la Bibliothèque nationale du Canada de reproduire, prêter, distribuer ou vendre des copies de cette thèse sous la forme de microfiche/film, de reproduction sur papier ou sur format électronique.

The author retains ownership of the copyright in this thesis. Neither the thesis nor substantial extracts from it may be printed or otherwise reproduced without the author's permission.

L'auteur conserve la propriété du droit d'auteur qui protège cette thèse. Ni la thèse ni des extraits substantiels de celle-ci ne doivent être imprimés ou autrement reproduits sans son autorisation.

0-612-60101-3

Canada

University of Alberta

Library Release Form

Name of Author: Gerald R. Beaudoin

Title of Thesis: Fiber Optic Based Tunable Diode Laser Gas Detector

Degree: Master of Science

Year this Degree Granted: 2000

Permission is hereby granted to the University of Alberta Library to reproduce single copies of this thesis and to lend or sell such copies for private, scholarly, or scientific research purposes only.

The author reserves all other publication and other rights in association with the copyright in the thesis, and except as herein before provided, neither the thesis nor any substantial portion thereof may be printed or otherwise reproduced in any material form whatever without the author's prior written permission.

April 17, 2000

Gerald R. Beaudoin

9013-99 st.
Edmonton, AB
T6E 3V6
Canada

University of Alberta

Faculty of Graduate Studies and Research

The undersigned certify that they have read, and recommend to the Faculty of Graduate Studies and Research for acceptance, a thesis entitled *Fiber Optic Based Tunable Diode Laser Gas Detector* by Gerald R. Beaudoin in partial fulfillment of the requirements for the degree of Master of Science.

Dr. John Tulip
Supervisor

Dr. C. E. Capjack

Dr. J. N. McMullin

Dr. J. Tuszynski

Date: April 17, 2000

Abstract

The development of a multiple detection site gas detector was undertaken. Using absorption detection via Tunable Diode Laser Spectroscopy [TDLS], a fiber optic light distribution system was assembled to supply several remote detection heads with atmospheric probing laser light. The system can be used for a wide variety of molecular species exhibiting absorption at wavelengths between 1.3 μm to 1.7 μm. The toxic gas Hydrogen Sulfide, H_2S, was chosen as the detection gas for this project because of potential uses in the petrochemical industry. Development and testing of a signal subtraction routine was undertaken in order to compensate for the presence of a stable absorption background. A sensitivity of ~ 10 PPMM is reached for the test H_2S absorption line.

For Heather,

Acknowledgements

I was fortunate to have the opportunity to work on this project under the direction of Dr. John Tulip. His words of wisdom provided direction and encouragement. There is no way for me to express the depth of experience I accumulated while working for him.

A sincere thank you is extended out to Mr. Ben Bathgate. Without his technical wizardry this project would never have been completed.

I must also thank all the machinists who built metal monsters from my sometimes incomprehensible CAD drawings. It was always a pleasure to work with such patience and understanding.

While learning how the GasFinder system functioned, Perry Kain and Jim Bauer were always there to answer my questions. A warm thanks to them and everyone else who helped at Boreal Laser Inc.

While working on this project, Dwayne Dickey was always there with his sobering observations and evaluations. Pushing the boundaries always seemed to be on the agenda and I thank him for his time and patience. I am especially grateful for his help in reviewing this manuscript.

Contents

	Page
1. Introduction	1
1.1 H_2S Safety	2
1.2 System Configuration	2
2. Laser Diode Controller	4
2.1 Tunable Diode Laser Spectroscopy	5
2.1.1 Ratiometric Gas Detection	13
2.1.2 H_2S Absorption Profile	15
2.1.3 Etalon Theory	17
2.2 Laser Diode Characteristics	21
2.3 Boreal Laser Inc. Transmitter	24
3. Fiber Optics	28
3.1 Optical Power Units	28
3.2 Fiber Propagation	30
3.2.1 Fiber Coupling	31
3.2.2 Fiber Collimation	34
I. Aspheric Lenses	36
II. Grin Lenses	37
3.2.3 Absorption	38
3.2.4 Dispersion	39
3.3 Optical Splitter	40
4. Remote Head	44
4.1 Design	45
4.2 Alignment Procedure	46

4.3 Beam Pointing 47
4.4 Retro-Reflector 48
4.5 Collection Optic 48
4.6 Pre-Amplified Detector 50
4.7 Beam Propagation 51
4.8 Turbulence 52
4.9 MultiMode Fiber Optic Link 53
5. Signal Processing 55
5.1 Analysis Electronics 56
5.1.1 Analog Switch 56
5.1.2 Boreal Laser Inc. Receiver 58
5.2 Reference Cell 60
5.2.1 Optical Test Base 60
5.3 On-line Processing 61
5.3.1 Standard On-line Processing 62
5.3.2 On-line Background Subtraction 64
5.4 Standard Off-line Processing 64
5.4.1 Off-line Background Subtraction 65
5.5 Signal Distortions 65
5.6 Results 71
5.6.1 Standard On-line Processing 71
5.6.2 On-line Background Subtraction 76
5.6.3 Standard Off-line Processing 77
5.6.4 Off-line Background Subtraction 79
5.7 Minimum Sensitivity 82
5.8 Calibration Error 83
6. Conclusions 84

References		88
Appendix A	Example Support Figures	94
Appendix B	Mathematica Simulation Programs	96

List of Tables

Table	Page	Description
1	27	Operating Conditions of Laser Diode for H_2S Gas Detection
2	30	Fiber Optic GasFinder Link Budget
3	34	Measured Connector Losses
4	36	Properties of the AC210T Aspheric Lens
5	38	Properties of the GRIN GLW8580-1550 nm Lens
6	41	Reference Cell Supply Splitter Properties
7	42	Remote Head Supply Splitter Properties
8	42	Probe Beam Supply Intensities
9	49	Off-Axis Parabolic Mirror Attributes
10	51	Beam Waist at various Propagation Path lengths
11	57	Analog Switch Specifications

List of Figures

Figure	Page	Description
1.0	3	System Block Diagram
2.0	8	WMS Theoretical Waveforms
2.1	9	Convergence Test Results for FMS
2.2	12	Model Signal obtained with FMS
2.3	13	Gas Signal Example
2.4	16	H_2S Absorption Profile
2.5	17	Etalon Model
2.6	18	Interference Pattern Created by a 1 cm Etalon
2.7	19	Fiber Etalon Model
2.8	20	Theoretical Etalon Noise Effects in TDLS
2.9	22	Optical Power Characteristics of the Laser Diode
2.10	23	Linearity of Laser Output vs. Injection Current Bias
2.11	26	Effect of RF Modulation Depth on Gas Signal Size
3.0	29	Calibration of System L.V. units
3.1	32	Types of Fiber Coupling Losses
3.2	33	Loss Dependance on Connector Mismatch
3.3	35	Fiber Emission Numerical Aperture
3.4	35	SingleMode Fiber Emission Characteristics
3.5	38	GRIN lens Collimation Example
3.6	40	Optical Coupler Connector Diagram
3.7	41	Fiber Optic Probe Beam Supply Network
3.8	43	Demonstration of Splitter TDLS Transparency
3.9	43	Effects of a Splitter on a Gas Signal
4.0	44	Remote Head Picture
4.1	45	Remote Head Block Diagram
4.2	49	Off-Axis Parabolic Mirror Diagram
4.3	51	Light Intensity vs. Signal Created by Pre-Amplified Detector
4.4	55	Light Intensity Test of Gas Concentration Stability
5.0	57	Analog Switch Channel Position
5.1	58	Receiver Block Diagram
5.2	59	Receiver Board Signal Calibration
5.3	63	Primary GasFinder Menu Layout
5.4		Deleted

5.5	67	Demonstration of Phase Noise Peaks
5.6	68	Unprocessed Waveform to Demonstrate Phase Noise
5.7	70	Stability of Imprinted Noise Structure
5.8	71	On-line Acquired Reference Signal Example
5.9	72	On-line Acquired Signal Example
5.10	73	On-line Processing 8000 PPMM Gas Test
5.11	74	Stability of Gas Readings
5.12	75	Standard On-line Processing Gas Detection Error
5.13	76	Online Background Subtraction Algorithm Testing
5.14	79	Raw Acquired Signal Calculated PPMM Readings
5.15	80	Background Subtraction Improvements on Signal Waveform
5.16	81	Wait Index Effects on a Sample Sets Average Gas Concentration
5.17	82	Background Subtracted Error in Calculated Gas Concentration
A.1	94	Operating Characteristics of the Fiber Options 175B Video Transmission Link
A.2	94	Operating Characteristics of the Link with the ZFL Amp. Before the Transmitter Input
A.3	95	Effect of Inaccurate Phase Shifter Setting on the Gas Waveform
A.4	95	Demonstration of the range of possible signal waveforms for all possible phase shifter settings.

List of Abbreviations

Abbreviation	Definition
DFB	Distributed Feedback
DSP	Digital Signal Processing
FFT	Fast Fourier Transform
FMS	Frequency Modulation Spectroscopy
GPIB	General Purpose Interface Bus
GRIN	Gradient Index
H_2S	Hydrogen Sulfide
HDTV	High Definition Television
HWHM	Half Width at Half Maximum
LED	Light Emitting Diode
LV	Light Value – system unit for signal strength
NMR	Nuclear Magnetic Resonance
PLL	Phase Locked Loop
PPM	Parts per Million
PPMM	Parts Per Million Metres
RAM	Residual Amplitude Modulation
SNR	Signal to Noise Ratio
TDLS	Tunable Diode Laser Spectroscopy
WMS	Wavelength Modulation Spectroscopy

1. Introduction

The development of precision pollutant measurement techniques has been spurred by society becoming more aware of the harmful effects of toxic emissions. Global warming trends have led to strict legislation dealing with pollution. In response, industry and governments alike are researching methods of quantifying and controlling toxic emissions.

A novel approach of measuring pollutant concentrations was developed in the early 80's. The technique uses a modulated laser diode that is tuned to the absorption peak. By monitoring the laser light intensity after it has passed through the atmosphere, an average gas concentration can be obtained for the path over which the light propagated. This technique, called Tunable Diode Laser Spectroscopy [TDLS], facilitated development of a gas detector that is more accurate and less sensitive to atmospheric mixing errors inherent in the older gas sampling techniques.

This thesis deals with the further development of this novel gas detection technique. As alluded to above, most present day gas detectors are hampered by the use of local measurement techniques. These systems take a small sample of air and analyze it using a variety of chemical techniques. While the data is reliable for the given sample, the readings do not indicate the average pollutant concentration within the area of interest.

The project outlined by this thesis incorporates Boreal Laser Inc.'s GasFinder. This patented system (US Patent 5,637,872) was modified such that it could sense gas along a number of optical paths by coupling the gas sensing laser light into a fiber optic distribution network. The entire system has the aim of detecting Hydrogen Sulfide, H_2S, along four or more optical paths.

1.1 H_2S Safety

The quest for a reliable H_2S detector is extremely important considering its toxicity and prevalence in the oil and gas industry. Before embarking on the relevant technology, a brief look at the safety issues associated with Hydrogen Sulfide, H_2S, will be provided.

Hydrogen Sulfide is a colourless gas that is slightly heavier than air. This means that it will preferentially collect in trenches and other low-lying areas. Humans are fortunate enough to have an on-board H_2S gas detector: the nose. Hydrogen Sulfide has a characteristic rotten egg smell, which is noticeable at less than 5 ppm. However, smell should never be relied upon since at concentrations above 150 ppm the olfactory sense is paralyzed leading to a false assumption that the gas is no longer present or has dissipated. Eye irritation will develop at concentrations below 50 ppm and after a few minutes at 100-200 ppm coughing fits will begin leading to pain in the respiratory tract. Being in an environment with an H_2S concentration above 500 ppm for 30 min will cause a loss of consciousness and possibly death [1,2].

The rapidity of effect and the fact that the gas can no longer be smelled at higher concentrations makes this gas as deadly as any known war gas. Those overcome by the effects of this gas should be removed from the area as soon as possible. Resuscitation should be performed immediately and the victim ought to be under medical observation for at least 48 hours after exposure. Treatment will, of course, depend on the severity of the exposure but medical attention should be sought whatever the case. That having been said, we will now move on to a discussion of the inner workings of the fiber optic H_2S gas detector built in this project.

1.2 System Configuration

When broken down to individual sub-components the entire detection system is basically an analog communication system. Principle sub-assemblies are the laser diode controller [Chapter 2], the fiber optic network [Chapter 3], the remote detection head [Chapter 4], the signal analysis electronics and signal processing [Chapter 5]. The following block diagram illustrates the principal functions of the Fiber Optic Based, Remote Detection Site Laser Gas Detector. A brief outline of the entire

system with references to the relevant sections is included here to provide both clarity and a thesis outline.

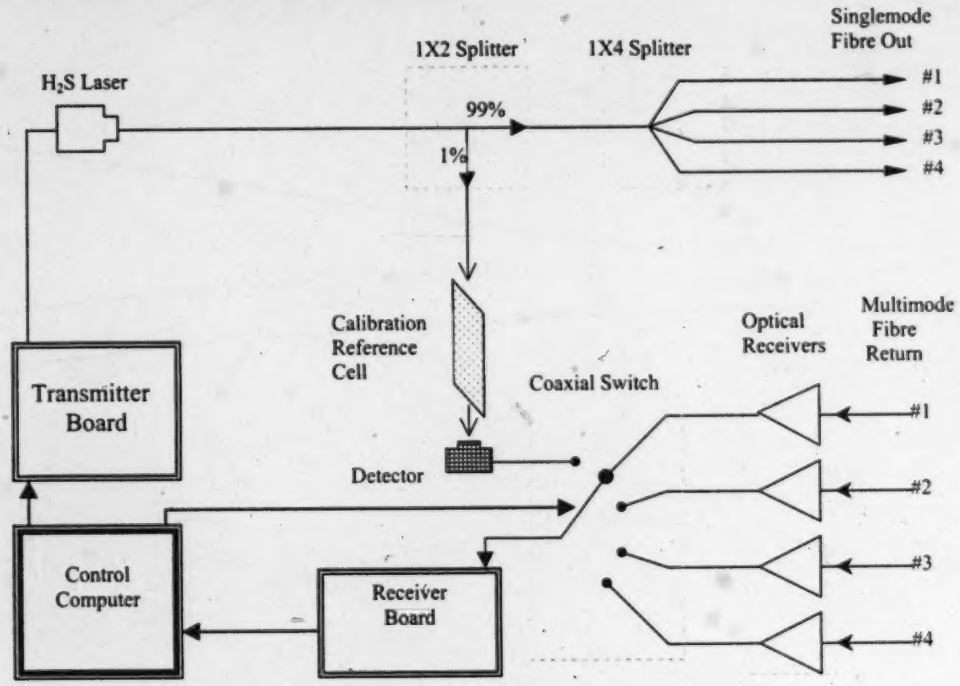

Figure 1.0 : System Block Diagram

The TDLS gas detection technique used in this project, described further in §2.1, requires extremely precise control over the laser diode. The Laser diode controller or transmitter is elaborated upon in §2.2. A description of the laser diode characteristics is included in §2.3.

Once the probe laser light is launched onto the fiber optic, the light travels down the distribution network to supply each detector head. The third chapter on Fiber optics discusses the important aspects of accomplishing light distribution. §3.1 provides the relevant optical power theory, while §3.2 discusses the effects of fiber propagation on the probe light. The optical splitter technology used to devide the probe light is defined in §3.3.

At each detection site, a remote detection head launches the probe beam. The beam then travels over the detection path of interest and is

reflected back to the detector head by a retroreflector, described in §4.4. The remote head design, discussed in §4.1, required knowledge of how the probe beam propagates within free space [§4.7]. The effects of turbulence are addressed in Section 4.8. Collecting the light after travelling over the path of interest and focussing it onto the detector element was accomplished using an off-axis parabolic mirror which is defined in §4.5. Once the light has been detected and the signal amplified, using the preamplified detector outlined in §4.6, the signal was then relayed back to the central system using a multimode fiber optic link that is defined in §4.9.

The use of modulation in the detection process requires some signal mixing to be performed by the signal analysis electronics defined in §5.1. Outlined in §5.1.1, the analog switch selects the detection path of interest, and checks the reference cell signal for a calibration measurement. The signal manipulation performed by the on-board computer, described in detail in §5.3, determines the detected gas concentration. This processing can also be achieved by passing the data to an off-line processing computer, as described in §5.4. Understanding the noise sources allows the minimum sensitivity of the entire instrument to be calculated as is done in §5.6.

Conclusions [Chapter 6], References and Appendices A-D conclude the thesis. The conclusions present over-all analysis along with further methods of system improvement. References are organized by number in order of appearance within the thesis. Appendix A includes support figures not included in the thesis. Mathematica notebooks used to generate the theoretical plots shown in the thesis are found in Appendix B.

2. Laser Diode Controller

As highlighted earlier, the Fiber Optic Based, Remote Gas Detector is basically an analog communication link. The only differing quality between the system developed and a classical communication link is that normally the information to be transmitted by the link is encoded at the transmitter, while here the information is imprinted on the signal by the link medium itself.

The crucial components of all communication systems are the transmitter, the link medium, and the receiver. In this system, the transmitter prepares the probe laser light such that optimal gas detection sensitivity will be achieved. Control of the laser diode operating temperature and injection current are crucial for noise free, reliable gas detection. The transmitter electronic board included in the Boreal Laser GasFinder is charged with the task of controlling the injection current of the laser diode. Some possible problems that may arise if this is done improperly are low light values, poor sensitivity and even a failure to detect gas.

2.1 Tunable Diode Laser Spectroscopy [TDLS]

The development of more accurate gas detection techniques was spurred by difficulties associated with common detection techniques. In the past, the primary method of detecting gas was by the use of a point gas chemical sensor. These sensors sample a small amount of air and perform a chemical analysis to determine its constituents and concentrations. It is assumed that the sample is a reasonable approximation of the surrounding environment. However, pockets of differing gas concentrations will not be seen by the sampling method. Another significant problem is calibrating these gas sensors. Using the knowledge that all molecules will absorb characteristic wavelengths of light allowed scientists to develop TDLS.

TDLS is a sensitive, calibrated gas detection technique. This section will endeavor to explain some of the theoretical underpinnings of the technique. TDLS is also referred to as Wavelength Modulation Spectroscopy [WMS] and Frequency Modulation Spectroscopy [FMS]. A discussion of the how these methods work follows. Determination of

the gas concentration is done with the ratiometric method described in §2.1.1. A look at the absorption profile used to detect H_2S is included in §2.1.2, while theoretical analysis of possible noise sources can be found in §2.1.3

The energy levels of a molecule are quantized and therefore the absorption of light will only occur at discrete, allowable energies. The mass of the constituent atoms, the strengths of their bonds and the angular momentum selection rules determine which photon energies and polarizations will be absorbed. When a molecule absorbs a photon of the correct energy it will jump into a rotational or vibrational excited state. By tuning the laser light over the characteristic absorption wavelength of a molecule, scientists were able to determine the concentration of gases by measuring the amount of light absorbed. The advent of the tunable diode laser allowed researchers to modulate the laser light at RF frequencies which achieved higher sensitivities.

It is well known that absorption causes the light intensity to decay exponentially with the distance the light travels [3,4]. The Beer-Lambert law describes the relation between the light intensity and absorption over a propagation path L. This law is given by:

$$I(\omega, L) = I_o e^{[-\alpha(\omega) P_a C L]}$$

Normally, $\alpha(\omega)\, P_a C L << 1$ and can, therefore, be approximated by:

$$I(\omega, L) \approx I_0 [1 - \alpha(\omega) P_a C L]$$

where ω denotes the angular frequency of the light, C is the concentration of the gas per atmosphere of pressure, P_a is the partial pressure of the gas in atmospheres (atm.), I_o is the incident light intensity and $\alpha(\omega)$ is the linear absorption coefficient in m^2/molecule. The absorption coefficient is given by $\alpha(\omega) = S \cdot g(\omega - \omega_0)$, where S is the molecular line intensity in meters/molecule, $g(\omega - \omega_0)$ is the normalized lineshape function (units of meters) and ω_0 is the linecenter frequency of the absorption profile. By scanning the frequency of the laser light over the absorption profile of the molecule, $\alpha(\omega)$, the intensity of the detected light will decrease to a

minimum at the linecenter, and return to a maximum value when the laser is on either side of the absorption profile.

The use of a tunable laser allows the profile of the absorption line for the pollutant molecule to be traced out by the laser as it sweeps over the line. This is accomplished by varying the injection current of the semiconductor laser diode. Since the refractive index of the semiconductor laser structure varies with the number of carriers in its valence band, the optical path length of the resonator cavity will change with injection current. This allows the emission wavelength of the diode to be scanned [5].

The injection current supplied to the Laser diode has the following form:

$$i_c(t) = i_{bias} + i_{ramp}(t) + i_{mod} Sin(\omega_m t)$$

where all currents are expressed in mA and i_{bias} denotes the injection current bias set point, $i_{ramp}(t)$ is the injection current ramp modulation and i_{mod} is the injection current RF modulation amplitude. The ramp modulation, $i_{ramp}(t)$, is a Sawtooth wave with a frequency of f_r= 354 Hz as described in §2.3. The ramp modulation is responsible for the wavelength scan over the absorption profile while the RF modulation is used to improve sensitivity through the harmonic detection technique.

Superimposing a low frequency modulation on the injection current of the laser is referred to in the literature as Wavelength Modulation Spectroscopy [WMS] [6,7]. Higher frequency modulations are designated as Frequency Modulation Spectroscopy [FMS] [6,7]. Other variations in detection and modulation methods have also been devised. Two closely spaced high frequency modulations have been used to provide a low frequency detection signal with the same sensitivity offered by using higher frequency modulations [8,9]. Changing the harmonic at which the incoming signal is analyzed also changes the noise rejection characteristics of the method and thus ultimate sensitivity [6].

Since the Boreal Laser GasFinder was incorporated into this project, the detection method (i.e. receiver board) was already defined. The Boreal Laser receiver detects the variation in received second harmonic amplitude over the wavelength scan. The RF modulation used by the Boreal Laser transmitter is at 10 MHz. Unfortunately this

modulation frequency is between the realm of WMS and FMS. Each method has strengths and weaknesses in predicting signal waveforms.

The simplest method of characterizing the important parameters in TDLS is the WMS analysis. An important weakness in this analysis is that the Residual Amplitude Modulation [RAM] noise imprinted on the scan of the laser as a result of the injection current modulation, is ignored. It is assumed that the laser exhibits only wavelength changes resulting from injection current modulations. We therefore assume the time dependence of the laser oscillation frequency as:

$$\omega(t) = \omega_0 + \beta \cdot i_{ramp}(t) + \beta i_{mod} Cos(\omega_m t)$$

where ω_0 the bias laser emission frequency, which is assumed to be set to the linecenter frequency, β is the frequency modulation depth in Hz/mA, and ω_m is the modulation frequency in radians/sec [7]. Because the modulation frequency, ω_m, is much larger than the ramp frequency, f_r, it simplifies the analysis to include the wavelength scanning ramp term in the optical carrier frequency. We therefore define the instantaneous scan laser frequency as $\omega_s(t) = \omega_0 + \beta i_{ramp}(t)$. This is effectively considering the emission frequency of the diode to include the ramp time dependence. We then expect the time dependence of the detected light intensity after traveling through the absorbing medium to have the form:

$$I(t,L) = I_0[1 - \alpha(\omega_s(t) + \beta i_{mod} Cos(\omega_m t))P_a CL]$$

By assuming that $g(\omega - \omega_0)$ is a Lorentzian absorption profile, we are able to expand $\alpha(\omega_s(t) + \beta i_{mod} Cos(\omega_m t))$ into a cosine Fourier series such that [10]:

$$\alpha(\omega_s(t) + \beta i_{mod} Cos(\omega_m t)) = \sum_{n=0}^{\infty} H_n(\omega_s(t)) Cos(n\omega_m t)$$

where $H_n(\omega_s(t))$ is the nth Fourier component of the modulated absorption coefficient. The solutions for the first harmonic, $H_1(\omega_s(t))$ and the second harmonic, $H_2(\omega_s(t))$, were calculated by Arndt for application in NMR [11]. Figure 2.0 plots the magnitude of $H_1(\omega_s(t))$ and $H_2(\omega_s(t))$ obtained using a model H_2S absorption profile, defined later in §2.1.1, versus the

scan frequency, $\omega_s(t)$, in GHz from the absorption linecenter. Further analysis of the WMS waveforms and their limits of applicability is given in the literature [6,7,10].

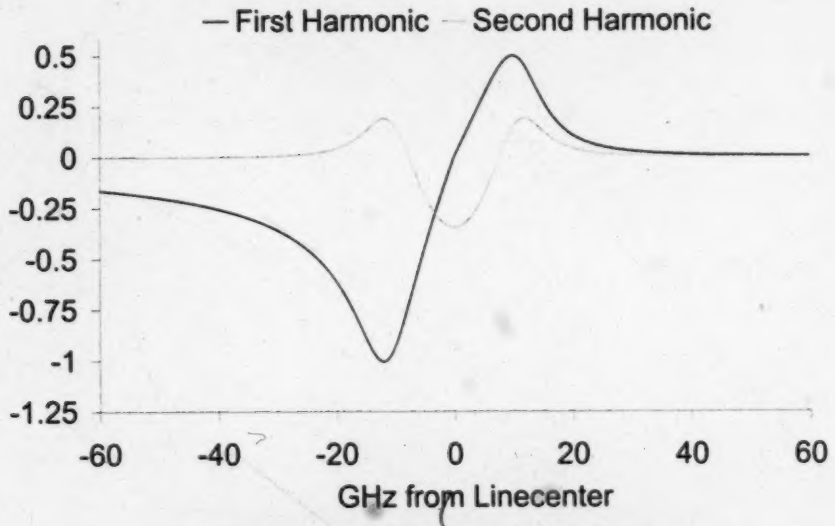

Figure 2.0 : WMS Theoretical Waveforms

The modulation frequency used in this project is between both the FMS and WMS domains and therefore both analytical methods provide insights. One strength of the FMS theory is that it is capable of determining how noise sources such as etalons, fiber reflection cavities, and RAM will effect system performance.

The FMS formalism relies on describing the imposed modulations with the electric field strength rather than stating the modulations in terms of the resulting optical intensity. Neglecting amplitude modulations as a result of the ramp, we begin by stating the electric field as [3,6,7]:

$$E(t) = E_0\left[1 + M\sin(\omega_m t + \psi)\right] e^{\left[i(\omega_s(t) + \beta i_{mod}\cos(\omega_m t))\right]}$$

where M is the amplitude modulation [AM] index, and ψ is the phase relationship between the amplitude modulation and the frequency

modulation. Because the intensity is proportional to the square of the electric field, the total intensity will be given by: $I(t) = I_0[1 + 2M\sin(\omega_m t)]$. Thus, the AM index is given by $M = \frac{|I_0 - I_{max}|}{2I_0}$ [6]. ψ has been shown to be π/2 at modulation frequencies less than 750 MHz [4,12,13]. The frequency modulation depth is denoted by β and is normally in the realm of 1 GHz/mA of injection current modulation [14].

We then use the Jacobi-Anger formula [15]:

$$e^{i(\beta i_{mod}\sin(\omega_m t))} = \sum_{l=-\infty}^{\infty} J_l(\beta i_{mod})\, e^{il\omega_m t}$$

to expand the electric field expression in a harmonic decomposition such that [6]:

$$E(t) = E_0 \sum_{l=-\infty}^{\infty} r_l\, e^{i(\omega_s(t)+l\omega_m)t}$$

where $r_l = -\frac{M}{2i}e^{-i\psi}J_{l+1}(\beta i_{mod}) + J_l(\beta i_{mod}) + \frac{M}{2i}e^{i\psi}J_{l-1}(\beta i_{mod})$ and J_l is the Bessel function of the first kind.

When this field is attenuated by a frequency dependent absorption profile, $\alpha(\omega)$, each harmonic of the field can be seen to be absorbed at its corresponding frequency, ie. $\omega_s(t) + l\omega_m$. We can then write the electric field strength at the detector as:

$$E(t, \nu_c) = E_0 \sum_{l=-\infty}^{\infty} r_l\, e^{i(\omega_s(t)+l\omega_m)t} e^{-\alpha(\omega_s(t)+l\omega_m)P_a CL}$$

The detector reads the intensity of the field and therefore we must square the electric field. The square-law detector will pick up intensity variations composed of all the harmonics of the modulating frequency. The electrical signal obtained by a lock-in amplifier at the harmonic n of the modulation frequency is [6]:

$$I(t) = 2I_0[\mathrm{Re}(Z(t))\cos(\theta) - \mathrm{Im}(Z(t))\sin(\theta)]$$

where, $Z(t) = \sum_{l=-\infty}^{\infty} r_l r_{l-n}^{*} e^{-[\alpha(\omega_s(t)+l\omega_m)+\alpha(\omega_s(t)+(l-n)\omega_m)]P_o CL}$ and θ defines the phase angle between the modulation frequency and the reference frequency of the lock-in.

It is important to note that the strength of the signal received at the detection harmonic n, is directly proportional to the intensity of light detected, I_o. Thus, we expect the signal size to increase with the optical intensity picked up by the detector. The amount of light detected will, therefore, needs to be accounted for in the calculation of perceived gas concentration. This is discussed further in §2.1.1. Later, in §5.1, it will be shown how the receiver manipulates the incoming signal, *I(t)*, to determine the light intensity detected and how it selects the appropriate detection harmonic. For the theoretical analysis, it is stated that the receiver board accepts only the second harmonic. Z(t) at the second harmonic is given by:

$$Z(t) = \sum_{l=-\infty}^{\infty} r_l r_{l-2}^{*} e^{-[\alpha(\omega_s(t)+l\omega_m)-\alpha(\omega_s(t)+(l-2)\omega_m)]P_o CL}$$

This formula allows us to predict the general form of the signal, I(t), produced by the GasFinder. Of course, it is computationally impossible to calculate this expression as the summation index will never approach infinity. Therefore a convergence test is necessary. Figure 2.2 demonstrates how the number of terms included in the summation affects Z(t). The convergence test was conducted assuming no absorptive gas in the optical path since $\alpha(\omega)$ is a simple function, whose value is independent of *l*. The number of sum terms used is defined by the largest value of *l* used in the summation.

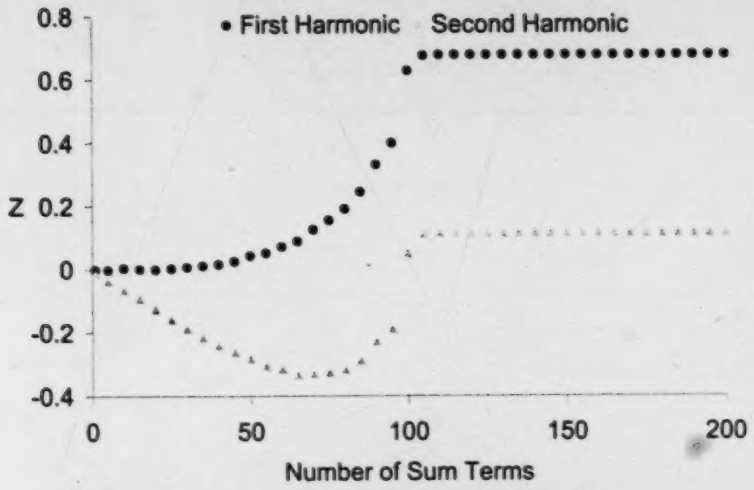

Figure 2.1 : Convergence Test Results for FMS

Normally in FMS the modulation frequency is much larger that 10 MHz and therefore fewer terms must be included in the analysis. Unfortunately, the 10 MHz modulation frequency chosen is in the gray area between FMS and WMS. This means that the summation must be carried out to a minimum of $l = \pm 100$.For the remainder of the FMS analysis it will be assumed that the series was only summed from $l = -110$ to $l = 110$.

Figure 2.3 demonstrates the second harmonic signal the FMS theory predicts with a theoretical lock-in phase setting of $\theta = 0$. The inclusion of RAM in the analysis leads to a non-zero average signal value. This bias has been investigated by a number of researchers [4,16,17].

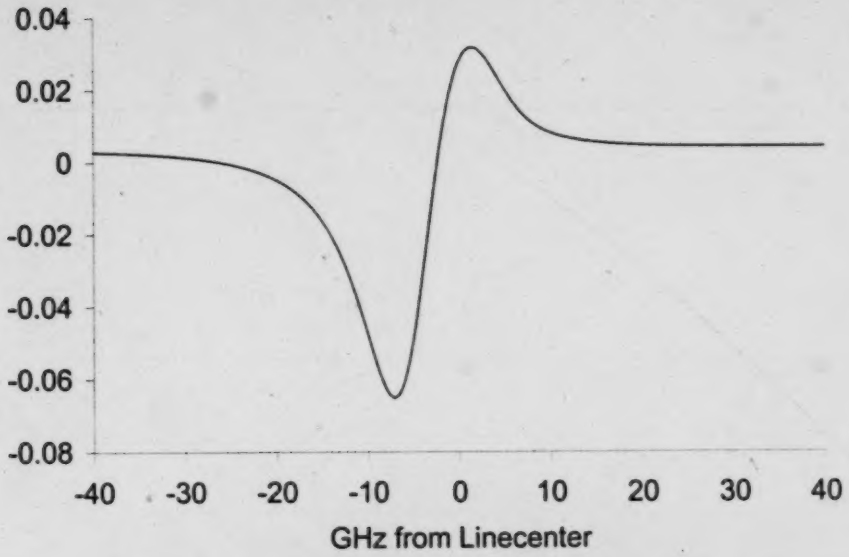

Figure 2.2: Model Second Harmonic Signal obtained with FMS

Figure 2.1 is an example of the signal generated by the Boreal Laser gas detection technique when the peak to peak size is a maximum and the asymmetry of the waveform is minimal. Figure A.3 in Appendix A shows that the gas waveform can be made to agree in form with the FMS predicted waveform with an appropriate phase shifter setting.

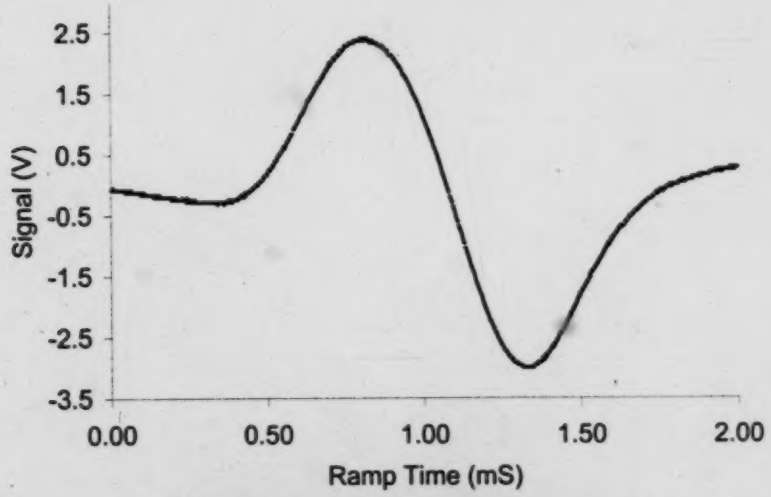

Figure 2.3 : Gas Signal Example

Another point of interest is how the signal peak depends on the frequency modulation depth, β. For a Lorentzian absorption profile the optimal modulation depth was defined by Arndt [11]. In his analysis, the optimal signal intensity will be reached when $\beta i_{mod} / \omega_{\Delta} \approx 2$ where ω_{Δ} is the Half Width at Half Maximum [HWHM] of the absorption profile. This conclusion has also been reached by various other researchers [3,4,6,7,16-18]. By setting the injection current modulation depth to the correct value, a maximum signal size will be achieved for a given gas concentration. The effect of modulation depth on signal size is demonstrated in Figure 2.11.

2.1.1 Ratiometric Gas Detection

The ratiometric gas detection technique allows analysis of the signal acquired to determine the gas concentration detected along an optical path. This is done by comparing the sample waveform with a reference waveform produced by a known gas concentration. When the probe beam is tuned to an absorption profile, it has been shown that the TDLS method will produce a characteristic waveform. Let us denote this normalized gas signal waveform as: $f(\omega_s)$, where ω_s denotes the optical scan frequency of the Laser diode. As the TDLS theory predicts, the signal amplitude depends on the intensity of light detected, *I*, the amount of absorbing gas present, *C*, and the length of optical path through which the light passes, *L*. For the reference signal all of these quantities are known. We can then express the reference waveform using the subscript *R* to denote reference quantities as:

$$S_R(\omega_s) = C_R L_R I_R f(\omega_s) \qquad 2.1.1(a)$$

There are two distinct possibilities for acquired signal waveforms. When no gas is present, the signal will be a flat line at zero and is written as $S_0(\omega_s) = 0$. The other possibility occurs when gas is present but we do not know the concentration. We state the waveform as:

$$S_1(\omega_s) = C_1 L_1 I_1 f(\omega_s) \qquad 2.1.1\ (b)$$

where C_1 denotes the unknown concentration of the gas.

In order to determine the unknown gas concentration, C_1, we use the fact that the amplitude of the gas signal depends linearly on the actual gas concentration. We, therefore, expect a linear relation between the two signals $S_R(\omega_s)$and $S_1(\omega_s)$. We define a proportionality constant m and state:

$$S_1(\omega_s) = m S_R(\omega_s) \qquad 2.1.1\ (c)$$

The replacement of S_{Sample} and $S_{reference}$ using 2.1.1 (a) and 2.1.1 (b) into 2.1.1 (c) leaves:

$$C_1 L_1 I_1 f(\omega_s) = m C_R L_R I_R f(\omega_s) \qquad 2.1.1\ (d)$$

After some algebra and the elimination of $f(\omega_s)$, we find:

$$C_1 = \frac{m\, C_R L_R I_R}{L_1 I_1} \qquad 2.1.1\ (e)$$

Therefore, the concentration of gas in a probe path can be determined by calculating the ratio, m. This ratio can be determined by simply using 2.1.1 (c) and averaging the value of m for each value of ω_s obtained. Determination of the constant of proportionality, m, can also be obtained by using a least squares fit.

Standard linear regression analysis uses N samples of two linearly related variables, (x_N,y_N). The data acquisition method in the gas detection system samples the waveform a number, N, of times over the scan. As we expect the probe path signal, $S_1(\omega_N)$, to be linearly related for each sample frequency, N, to the reference signal, $S_R(\omega_N)$, as was stated in 2.1.1 (c). The slope, m, can then be calculated using [55]:

$$m = \frac{N\left(\sum_N S_R(\omega_N) S_1(\omega_N)\right) - \sum_N S_R(\omega_N) \sum_N S_1(\omega_N)}{N\left(\sum_N S_R(\omega_N)^2\right) - \left(\sum_N S_R(\omega_N)\right)^2} \qquad 2.1.1\ (f)$$

When no gas is present, $S_0(\omega_s) = 0$, m will take a value of zero only if $S_R(\omega_s)$ is anti-symmetric. This is normally the case when the phase shifter of the receiver is set properly.

As an aside, it is instructive to consider what result the ratiometric calculations will give for an input signal that is the negative of the reference cell gas signal. In this case we express the sample signal as:

$$S_1(\omega_s) = C_1 L_1 I_1 \bullet -f(\omega_s) \qquad 2.1.1\ (g)$$

When this is substituted into the linear fit assumption as before, we are left with:

$$C_1 = \frac{-m\, C_R L_R I_R}{L_1 I_1} \qquad 2.1.1\ (h)$$

We therefore expect a negative concentration when a waveform that is the negative of the reference waveform is obtained by the sample arm. This will never occur for a gas signal, but can occur for noise imprinted on the waveform. This possibility is discussed further in §5.6.

2.1.2 H_2S Absorption Profile

It should be noted that any molecular species with absorption lines in the 1.3 μm to 1.6 μm region may be detected by this system, assuming the laser diode is chosen to emit at the desired absorption wavelength. This window in TDLS detection is limited by the transparency of the fiber optics used in the project. Outside this window, the fiber glass will exhibit losses due to absorption which would limit the distance at which remote detector heads could be positioned.

Because of the potential uses in the petrochemical industry, Hydrogen Sulfide, H_2S, was chosen as the standard detection gas for this project. H_2S is one of the more difficult gases to detect because of the proximity of the abundant Carbon Dioxide, CO_2, absorption lines and the relative weakness of its absorption lines.

The H_2S absorption spectrum has been mapped out in the 1.6 μm spectral region [19]. This three atom molecule has three vibrational degrees of freedom. The strongest of the molecular absorption spectra in the wavelength region we are interested in correspond to the rotational spectra of the $2\nu_1+\nu_2$ and $\nu_1+\nu_2+\nu_3$ vibrational states [20]. Another criterion used for the choice of absorption line was the proximity to the lines of other gases which may be present in the natural environment. These include H_20, CO_2, CO, O_2, and OH. The absorption line chosen is at 1.57776 μm and corresponds to the (211) rotational level of the $2\nu_1+\nu_2$ vibrational state in the predominant $H_2{}^{32}S$ molecule. For $H_2{}^{34}S$, the (221) rotational level of the same state is situated at 1.57779 μm, which likely contributes to this spectral line being the most absorptive for this molecule. The Voigt profile self broadening coefficient for H_2S is 0.175 cm^{-1} atm^{-1}. [19] A plot of the Lorentzian broadened absorption profile used in this project is indicated in Figure 2.4.

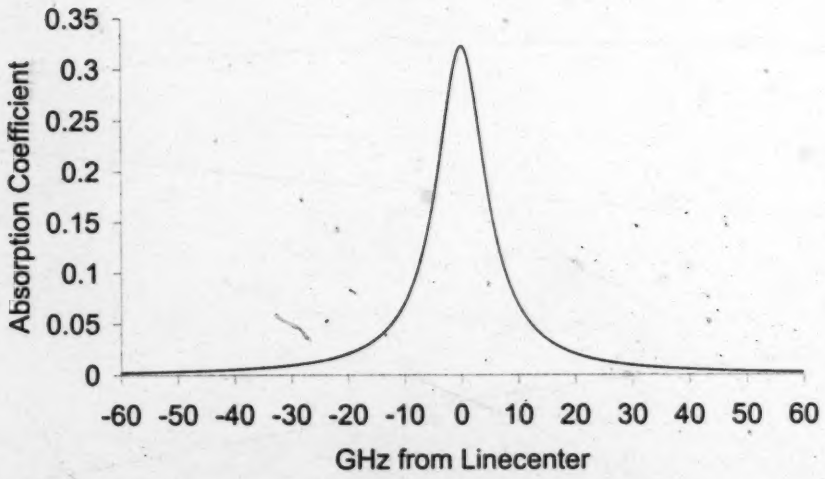

Figure 2.4: H_2S Absorption Profile

2.1.3 Etalon Theory

Another important phenomenon that must be understood when using TDLS for gas detection is the noise caused by etalons. In order to manipulate the probe light, it is necessary to use optical elements which

will cause distortions in the detected signal. This section will describe the theory involved in etalon phenomena. The observation of etalon fringes is shown in §5.5.

As the probe beam travels through the system it will necessarily pass through various optical elements. The Fresnel reflection equation predicts the relative intensities of both the reflected and transmitted light when light passes through an optical element. The relative amounts depend on both the angle of incidence relative to the interface normal and the indices of the differing media [21].

When a beam of light encounters an optical element, multiple reflections occur between the end faces. These reflected beams superimpose after each has acquired a phase shift as a result of the extra path length traveled within the optical element. This phenomenon is portrayed in Figure 2.5

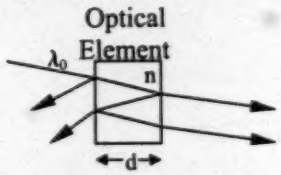

Figure 2.5: Etalon Model

Figure 2.5 exagerates the angles to display the reflected rays more easily. The issue of importance is that the phase shifted, reflected rays will interfere with the original ray. Each succesive ray will suffer a phase shift of $\delta = \frac{4\pi\, n\, d \cos\theta_t}{\lambda_0}$, where n is the index of the element that the multiply reflected rays travel within, θ_t is the transmission ray incidence angle with respect to the interface normal. When all of these phase shifted rays are made to interfere either by a detection process or a lens, there will be an interference effect causing a variation of the transmitted light intensity. The actual form of the ratio of the transmitted intensity to the incident intensity is given by the Airy function [22]:

$$\frac{I_t}{I_i} = \frac{1}{1+\left(\frac{2r}{1-r^2}\right)^2 \sin^2\left(\delta/2\right)}$$

where r denotes the amplitude reflection coefficient for the interface, ie $r^2 = \%$ light reflected at an interface. Plotting this variation of light

absorption over the wavelength sweep of our H_2S gas detector demonstrates how an etalon might cause a false gas-like signal in a TDLS system.

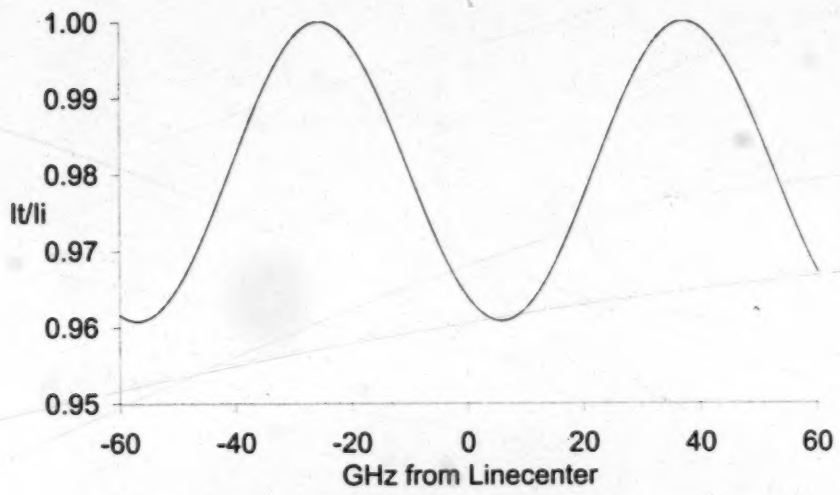

Figure 2.6: Interference Pattern Created by a 1 cm Etalon

Figure 2.6 was generated using a glass etalon with n=1.5 assuming a ~ 1 % reflection coefficient at a glass-glass interface. The amount of reflection determines the magnitude of the interference pattern, while the length of the etalon determines the frequency of the transmission oscillations. The important point to be gleaned from this graph is that etalons of this sort cause an absorption that depends on wavelength, which is exactly what is being detected by TDLS.

The above analysis illustrates the importance of avoiding optical elements such as lenses and glass windows. However, it has been shown that the multiple reflection and interference conditions needed to produce these interference fringes can occur in virtually any optical set-up whether the system is entirely free space or based on the use of fiber optics [24-30]. While the simple etalon theory provides a qualitative understanding of how this phenomenon can degrade system sensitivity, it fails in describing fiber optic based interference fringe production.

Using the formalism of FMS, we can state that the electric field of the clean laser probe beam is written as [6]:

$$E(t) = E_0 e^{i\omega_0 t} \sum_{l=-\infty}^{\infty} r_l e^{il\omega_m t}$$

where ω_0 is the carrier optical frequency, r_l is a constant containing the RAM and harmonic decomposition coefficients, and ω_m is the modulation frequency. If this probe beam were launched into a fiber optic system or a free-space optical system we would expect some interference fringes to appear due to multiple reflections within or between optical elements. The following figure demonstrates how an interference cavity might be set-up in a fiber optic system.

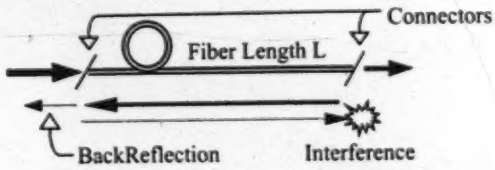

Figure 2.7: Fiber Etalon Model

Interference cavities occur in fiber optic systems via the backreflections that occur at fiber interfaces. The amount of backreflection and hence interference fringes, depends on the type of connector used as well as the fiber type. The creation of an interference pattern or fringe relies on the mixing of phase delayed light with another coherent light beam. The backreflections outlined in Figure 2.7, provide the phase delayed light necessary for interference. After the superposition of the light at the interface, the output light field will not have the same form as above. Assuming the fiber system in Figure 2.7, we can restate the output as [23]:

$$E_{out}(t) = E_0 \eta^2 \left[e^{i\omega_0 t} \sum_{l=-\infty}^{\infty} r_l e^{il\omega_m t} + \alpha_1 \alpha_2 e^{i\omega_0 (t+\tau)} \sum_{l=-\infty}^{\infty} r_l e^{il\omega_m (t+\tau)} \right]$$

where η denotes the loss of one connector, α_1 and α_2 are the backreflection coefficients for the first and second connectors respectively. We find the phase shift τ to be: $\tau = \frac{2Ln_0}{c}$ where L is the length between connectors, n_0 is the index of the fiber core and c is the speed of light in vacuum.

Using the above equations, Figure 2.8 was created to determine how various etalon thicknesses might create first and second harmonic distortions. The predicted noise is plotted in Figure 2.8. The signals created assume no gas is present and are only valid for the wavelength region of the H_2S absorption. The FMS theoretical analysis needed to calculate etalon contributions for other wavelength domains is included in Appendix B. It is important to note that the signal size is much smaller than the signal given for gas like signals. However, this graph clearly demonstrates that glass windows with a thickness between 5 and 20 mm could cause significant signal distortions if the reflectivity of the end face etalon is higher than the 1% assumed.

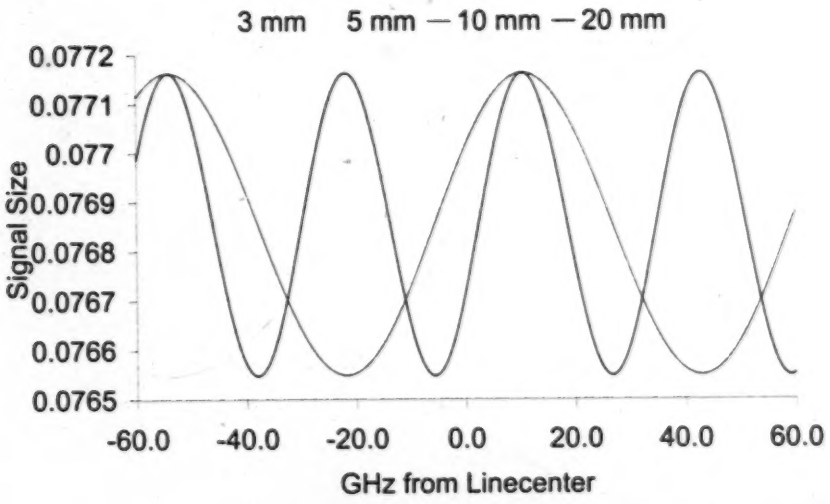

Figure 2.8: Theoretical Etalon Noise Effects in TDLS

While Figure 2.8 demonstrates how an etalon might cause noise in the system, many of the parameters used to generate the figure were outside the normal range of validity. First, the backreflection coefficients must be assumed to be much larger than they are in reality in order to produce large signal distortions. Secondly, the length of the fiber optic creates extremely high frequency noise contributions, which are difficult to reliably calculate. A third inaccuracy is the assumption of a completely coherent light source, which retains its coherence for all time.

However, the scientific literature provides examples of the prediction and demonstration of the existence of fiber optic interferometric noise in TDLS systems [23,24,31]. These examples

demonstrate that this noise limits the fundamental sensitivity in fiber optic systems but that a judicious choice of RF modulation depth can keep the interferometric noise at a minimum [23,24]. Further analysis of the etalon and interferometric noise phenomena is included in section 5.5 on signal distortions.

2.2 Laser Diode Characteristics

Diode lasers are not only used in spectroscopy but also in the communication industry. This intense commercial interest has initiated extensive research and product development leading to an explosion of possible uses for these novel lasers. Developments in diode laser technology have led to long lifetimes, narrow emission linewidths and high optical outputs, all of which are advantageous to the spectroscopy and communications industries.

The important diode characteristics for TDLS include the output power, the linearity of the output power vs. injection current, modulation effects on wavelength, the laser linewidth, and the temperature wavelength tuning characteristics. The importance of each of these characteristics is elaborated upon in the following section. The data given are all for the H_2S detection laser diode used in this project. The Laser used is a LD6204 manufactured by GEC-MARCONI Materials Technology Ltd [32].

The amount of laser diode output defines the absolute maximum number of gas detection sites. The laser light, after being coupled into a SingleMode fiber optic, is divided into several fibers by the splitter, described in §3.3. For sensitive gas detection, a minimum amount of light, ~ 1 mW, must be launched for the detector to receive enough light to function in a noise free region. The relation between the laser diode injection current and optical output produced by the particular laser diode used in this project is shown below. While Figure 2.9 demonstrates that higher optical power outputs can be achieved by simply using larger injection currents, the linearity of the curve is important for minimal modulation distortion and therefore gaining higher output powers through high injection currents is not advantageous. It is therefore important to purchase the laser diode with the highest possible output in order to obtain maximal output with minimal signal distortion.

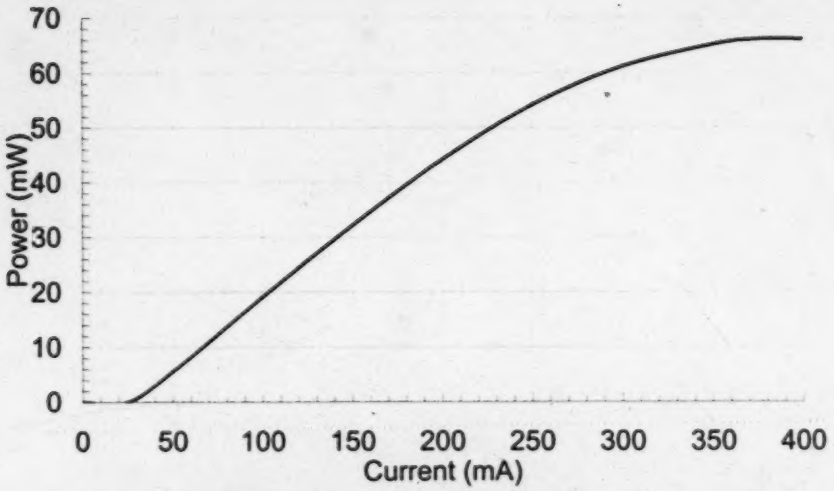

Figure 2.9: Optical Power Characteristics of the Laser Diode

The threshold current for this diode laser is 28 mA. This defines the minimum injection current needed to induce laser oscillation in the diode. A low injection current threshold keeps the possibility of laser clipping to a minimum. Laser clipping occurs when the injection current falls below the threshold as a result of modulations. The laser used in this project and most modern diode lasers have small threshold currents because of the use of strained layer quantum wells in their laser structure.

As aforementioned, the laser must be operated in a linear portion of the power relation for sensitive gas detection. Assuming a biased injection current, the optical power can be expanded as a power series around the bias point. This gives:

$$P = < P > + \frac{\partial P}{\partial I}(I - < I >) + \frac{1}{2}\frac{\partial^2 P}{\partial I^2}(I - < I >)^2 + \frac{1}{6}\frac{\partial^3 P}{\partial I^3}(I - < I >)^3 + \quad \ldots$$

The terms proportional to the square or cube of the injection current will lead to harmonic distortions in the optical power output [5]. These distortions in the probe light lead to noisy operation and ultimately poor sensitivity. However, choosing to operate the laser diode in the most linear region of the curve easily minimizes this. Figure 2.10 shows the manufacturer included linearity specifications of this projects laser diode. Note that the optimal operating injection current is 100 mA leading to a total output of 20 mW.

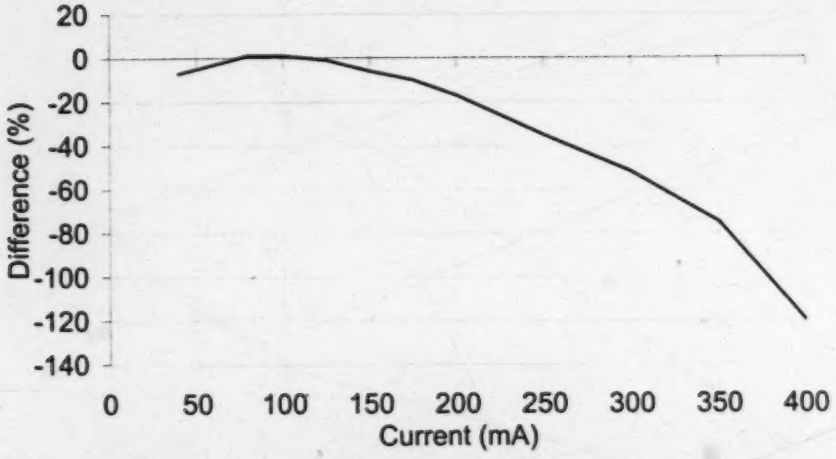

Figure 2.10: Linearity of Laser Output vs. Injection Current Bias

The wavelength tuning characteristics of the laser diode are important to determine injection current modulation required for optimal sensitivity. It is known that in order to detect gas, the wavelength of the laser must be swept across the absorption profile of the gas of interest. This wavelength sweep is created via a slight thermal effect within the laser diode structure. The reader is referred to a text by K. Petermann, Laser Diode Modulation and Noise, for further information about how the wavelength or frequency of a laser diode is modified by injection current changes [5]. It is generally excepted that DFB laser structures exhibit ~ 1 GHz of optical frequency change per mA of injection current modulation [14]. It should be noted here that the frequency dependence of the Laser on injection current also causes chirp which is undesirable for TDLS systems [31]. Chirp is defined by a change in the frequency tuning coefficiten with respect to the injection current. Unfortunately, this noise source is inherent to the Laser and nothing can be done to eliminate or reduce it. For most cases, however, the noise contribution from chirping effects is well below the etalon noise problems outlined earlier.

The center wavelength of the laser diode with an injection current of 150 mA is specified at $\lambda_c \approx 1576$ nm. This emission wavelength of the laser can be manipulated via temperature changes. A temperature

induced refractive index variation in the resonator cavity leads to a cavity optical path length change, causing the resonator to emit at a slightly different wavelength. A temperature change of 1°C will change the output wavelength to change by 0.1 nm for the style of laser diode used in this project.

For spectroscopic uses it is important that the laser diode is single mode; that is, the linewidth of the laser must be much narrower than the absorption profile of the gas to be scanned. This criterion is easily satisfied using a DFB laser cavity resonator structure. The linewidth of a typical absorption line is ~ 60 - 600 MHz [18], and laser diodes have a linewidth that is normally much smaller than 50 MHz. Modern laser diode linewidths will not be a problem in TDLS systems [32].

In the past, the phenomenon of laser diode mode hopping was a considerable headache in gas detection applications. Mode hopping occurs when the laser diode jumps resonator modes causing a drastic emission wavelength change. This problem was solved by extensive research and development performed by the communications laser diode industry.

2.3 Boreal Laser Inc. Transmitter

As was stated earlier, this system includes portions of the Boreal Laser GasFinder within its structure. The Boreal Laser Transmitter board was used to control the fiber coupled laser diode for this project.

For gas detection to occur, the injection current of the Laser Diode must be biased while a ramp modulation causes the diode emission wavelength to sweep over the gas absorption profile while simultaneously a 10 MHz modulation increases sensitivity. These requirements are met by using a hybrid of a commercially available laser diode driver and a 10 MHz oscillator coupled to the diode inputs using a bias tee.

The laser diode driver used by Boreal Laser is the LDD200-1P manufactured by Wavelength Electronics [33]. This driver is capable of functioning in constant optical power or constant injection current mode. A constant current is used here, since the injection current must be held at

its bias point to assure noise free operation. It must be remembered that bias injection current changes cause wavelength drift in the Laser diode.

The Wavelength Electronics driver is capable of supplying a 200 kHz modulation of the injection current via an external modulation input [33]. A sawtooth wave with a variable depth of modulation is created on the board and is supplied to the external modulation input causing a ramp in the injection current of the laser such that the wavelength is swept across the gas absorption line. The Boreal Laser Transmitter uses a 354 Hz ramp modulation. The magnitude of the ramp modulation determines the range over which the wavelength of the laser is swept. Therefore we can state that $\Delta\lambda \propto \frac{1}{\Delta i_r}$, an increased injection current changes the operating wavelength of the laser. Therefore if the depth of ramp modulation becomes larger, the width of the absorption profile will appear narrower in TDLS systems. The injection current ramp should therefore be chosen such that the width of the gas detection signal is larger, leaving less wavelength sweep for other background gas absorption lines or false signals from etalons. A 28 mA ramp modulation depth seemed to be the best use of the signal sweep available for computer analysis.

The frequency modulation of the injection current is provided using a 10 MHz crystal oscillator which is included on the transmitter board to provide clean oscillation. It is imperative that this signal be extremely clear with small higher order harmonic distortions since this will degrade the sensitivity of the instrument. The output of this oscillator is amplified and then overlaid onto the diode anode and cathode via the bias tee. A variable resistor changes the amount of oscillator amplification, thus controlling the depth of frequency modulation. This modulation depth must be sufficient to produce the largest possible signal.

The optimal modulation depth is found when the frequency modulation index is 2.2 times the HWHM frequency of the gas of interest [4,6,7]. Figure 2.11 demonstrates this dependence experimentally and was used to choose the optimal operating conditions. It should be noted that the received signal size will increase with the intensity of light detected by the photodiode. Therefore, a constant portion of the Laser diode output was aimed directly onto the detector photodiode. For this

figure, the received signal strength was determined by measuring the peak to peak voltage of the 10 MHz signal originating from the pre-amplified detector module discussed in §4.6. The Laser Transmitter board designed by Boreal Laser Inc. is only capable of a RF modulation current of 3.5 mA. This board was modified such that the maximum modulation depth was increased to ~ 7.6 mA. The amount of frequency modulation depth obtained by a DFB laser diode is ~ 1 GHz/mA [14]. Using Figure 2.11, the RF modulation depth was set to 7.5 mA.

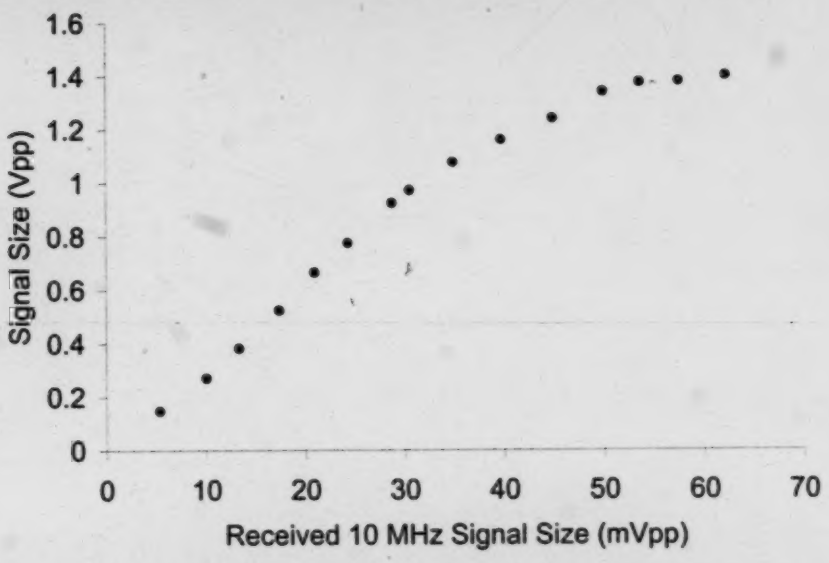

Figure 2.11: Effect of RF Modulation Depth on Gas Signal Size

The Boreal Transmitter board also controls the temperature of the diode such that the diode emission wavelength is stable. A Hytek Microsystems thermoelectric cooler controller stabilizes the temperature of the heat sink via two thermoelectric coolers, and hence the attached diode. A Marlow Industries bead thermistor [34] is epoxied into the heat sink to provide a temperature reading via resistance changes. A variable resistor on the transmitter board provides a set point resistance which is then compared to the thermistor resistance. The controller then determines if the heat sink must be warmed or cooled. A feedback loop within the controller helps to decide when it should supply the thermoelectric coolers with a current which modifies the temperature of the heat sink until the set point resistor and the thermistor are of equal resistance. A warm-up period of 3-5 minutes is normally required on system start-up to stabilize the Laser diode emission wavelength to the

absorption peak of the gas. For the Laser diode used in this project, the thermistor comparison set point resistance is set to 2.7 kΩ or equivalently 57 °C.

During the instrument warm-up, the thermoelectric coolers consume a great deal of power to quickly reach the temperature set point. The Hytek controller is capable of a maximum power dissipation of 6 W [35]. Thus during the initial warm-up the transmitter section draws up to 2 A and then once the temperature has been stabilized the current draw will drop to normal levels, ~ 200 mA.

To summarize the laser operating conditions that are maintained by the transmitter section the following table is included.

Operating Conditions of Laser Diode for H_2S Gas Detection	
Bias Current:	116 mA, 22 mW Light out
Ramp Frequency:	354 Hz Sawtooth wave
Ramp Depth:	3.8 mA Peak to Peak
Modulation Frequency:	10 MHz Sinusoidal wave
Modulation Depth:	7.5 mA Peak to Peak
Operating Temperature:	57 °C

Table 1

3. Fiber Optics

Fiber optic cable was initially developed in the early 1970's. Since then the technology has become widespread and now fiber optics span the world handling virtually all our communication needs. With this extensive communications backbone has come a wealth of knowledge about fiber optic technology. Therefore, the reader is directed to any of a large number of books on fiber optics for further information [36-41].

The modulated laser diode provides a relatively stable light output which is coupled into a short section of SingleMode fiber (q.v. §2.3). The light from this fiber then passes through connectors and splitters on its way to each of the remote detection sites. Discussion of losses associated to the connectors is found in §3.2.1 while the splitter is left to §3.3.

3.1 Optical Power Units

While working on this project, much confusion arose over the units used to define the amount of optical power carried within the optical fiber. Traditionally telecommunications engineers use the decibel system, which allows losses to be expressed easily. However, scientists use the conventional SI unit of Watts, normally mW. Some technical specifications are defined in the SI system, such as Laser Diode outputs, while specifications for communications equipment such as optical splitters and connectors are defined using decibels.

The Boreal Laser GasFinder also has its own measure of the light intensity detected: Light Value [L.V.]. The Light Value is derived as a measure of the amount of 10 MHz signal received by the receiver electronics, which is proportional to the amount of light detected.

Measurements of the optical power within the optical fiber were performed using a FIS OV-PM power meter calibrated at 1550 nm. As the wavelength of the probe beam is actually at 1578 nm, the intensity readings will be slightly larger than in reality since Ge semiconductor detectors have a maximum responsivity at 1500 nm and are less responsive at longer wavelengths.

Calibration of the Light Value unit system was performed by aiming a collimated laser beam of a known intensity onto the pre-amplified detector (described in §4.6) and obtaining the corresponding Light Value. This allowed the L.V. units to be calibrated to the accepted SI units of μW. The following figure demonstrates that the L.V. received corresponds to the same amount of detected light for both the remote head and the reference arm.

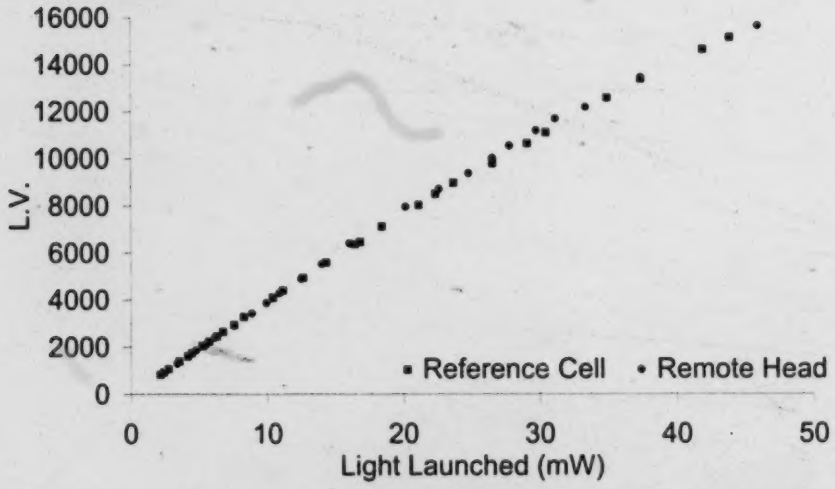

Figure 3.0: Calibration of System L.V. units

The decibel is a measure of the power ratio between an input beam with power P_1 and an output beam with power P_2:

$$dB = -10Log\left[\frac{P_2}{P_1}\right]$$

Expressing optical power in the decibel system, which is used in most loss measurements, uses 1 mW as the reference optical power P_1 in the above equation. The unit of optical power is then referred to as the dBm. Defined as:

$$dBm = 10Log\left[\frac{P_2}{1\,mW}\right]$$

If we consider our 10 mW fiber output Laser diode, we could then refer to it as having a 10 dBm output. Using this definition of optical power allows the losses of the system to be directly subtracted.

A system fiber optic link budget is easily calculated by subtracting the various losses from the fiber coupled Laser output. Care must be taken since the fiber optic industry has abandoned the negative sign on losses, assuming that the loss must be subtracted. Table 2 shows how the link budget in dB was calculated for the Fiber Optic Based GasFinder. Figure 3.7 illustrates the fiber optic network and its components.

Fiber Optic GasFinder Link Budget

Fiber coupled Laser output	10 dBm
Loss at connector 1	-0.3 dB
Drop at reference supply splitter	-0.07 dB
Loss at connector 2	-0.3 dB
Drop at 1X4 equal splitter	-6.7 dB
Loss at connector 3	-0.3 dB
Total probe light at each supply	2.33 dBm

Table 2

3.2 Fiber Propagation

Light propagates within a fiber optic in modes which satisfy Maxwell's Electromagnetic Equations. The number of possible solutions to these equations determines the number of modes propagated within the fiber core. This thin wire of glass is manufactured such that the index of refraction within the center of the fiber is greater than the index of the cladding surrounding it. The number of modes allowed to propagate depends on the diameter of the fiber and the relative index of refraction differences between the cladding and the core. Large diameter fiber, > 20 μm, normally supports hundreds of possible propagation modes, an is therefore referred to as MultiMode fiber. SingleMode fiber is only ~ 9 μm in diameter and only supports one mode of propagation.

The most important characteristics of fiber optic cable are the attenuation of the carried light signal and the dispersive effects of the fiber. In a TDLS gas detector system, the amount of attenuation or loss

within the fiber system limits both the number of remote detector heads as well as the distance at which these detection sites can be placed from the central system. However, losses can be minimized by careful fiber network design. Fiber optic dispersive effects limit the optical bandwidth available for a given fiber and are one of the limiting factors on the bit rate in digital communication links. For this project however, the gas sensing mechanism relies on analog modulation of the laser to detect the gas. The dispersion effects relating to analog modulation are discussed further in §3.2.4.

3.2.1 Fiber Coupling

The development of any fiber optic gas detection technology relies on being able to couple the Laser diode emitted light into fiber optic. Considering that the light travels within a ~ 9 μm core of a SingleMode fiber optic, this is a considerable task which requires precise aiming and fine tolerance focusing.

The first step in fiber coupling is to collect the light launched from the laser diode into a SingleMode fiber optic. This is a sensitive and crucial step in the system. Optimal system performance depends on noise free coupling, high coupling efficiency and proper isolation. Because of the relative importance and considerable experience necessary to accomplish efficient laser to fiber coupling, the laser was coupled to the fiber by Barry Zhang at Princeton Optics Inc.. Angle cut GRIN lenses were used to collimate and focus the emitted Laser light onto a SingleMode fiber with an efficiency of ~50 %. A polarization based isolator was placed between the GRIN lenses to stop backwards propagating light from entering the laser resonator.

Fiber to fiber coupling occurs at the interface between the various fiber optic elements in the system. The loss associated with a connection between two fibers is one of the most important losses in this system. In the case of SingleMode fiber, the light propagates within a central ~ 9 μm core, and therefore alignment requires both precision and care. Precision is required, since a slight mismatch will cause a good deal of excess loss. Cleanliness of the fibers is necessary because a speck of dust could conceivably block 50% of the light.

The principle difficulties associated with fiber to fiber coupling are: lateral offset, fiber face separation and angular tilt, between the fibers. Lateral offset occurs when the fibers are not precisely lined up. Losses due to end face separation occur because the laser beam will expand slightly within the gap between the fibers leading to losses on the outer edges of the beam. The relative angular tilt between fibers will cause losses as a result of the beam hitting the fiber end face outside the mode field acceptance angle of the fiber. These three possibilities and the formula for the loss that they incur is outlined in the Figure 3.1 [42].

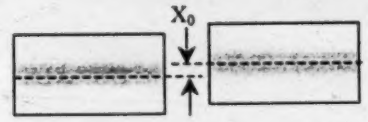

$$L = -10Log\left[e^{-\left(\frac{X_0}{w}\right)^2}\right]$$

(a)

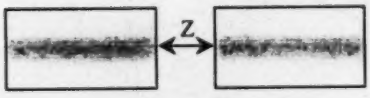

$$L = -10Log\left[\frac{1}{\left(\frac{z\lambda}{2\pi n_0 w^2}\right)^2 + 1}\right]$$

(b)

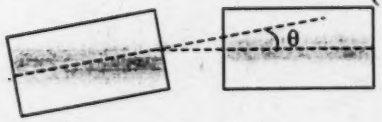

$$L = -10Log\left[e^{-\left(\frac{\sin\theta}{\lambda/n_0\pi w}\right)^2}\right]$$

(c)

Figure 3.1: Types of Fiber Coupling Losses
Loss stated in dB as a result of (a) lateral offset, (b) end face separation, and (c) angular tilt, where λ is the wavelength, n_o is the index of the medium between the fiber faces, and w is the mode field diameter of the fiber assuming both fibers are of equal mode field diameter [43].

A more realistic fiber coupling situation would have a combination of these alignment difficulties. The loss associated with several alignment mismatches is given by [43]:

$$L = -10Log\left[\left(\frac{4D}{B}\right)e^{-AC/B}\right]$$

where $A=\frac{(kw_1)^2}{2}$, $B=G^2+(D+1)^2$, $D=\left(w_2/w_1\right)^2$, $F=\frac{X_0}{kw_1^2}$,

$G=\frac{2Z}{kw_1^2}$, $k=2\pi n_0/\lambda$, $C=(D+1)F^2+2DFG\sin\theta+D(G^2+D+1)\sin^2\theta$

and w_1, w_2 are the mode field radii of the two fibers in the connector.

Only the extrinsic fiber positioning problems have been included. Such intrinsic difficulties as mode field diameter mismatch, fiber index profile mismatch, Fresnel reflection losses and core eccentricity flaws cannot be altered and are inherent difficulties within the coupling process.

The following figures demonstrate the relative importance of each type of extrinsic connector mismatch. These graphs demonstrate that lateral offset and angular alignment errors will have the most prominent effect on coupling efficiencies. Figure 3.2d shows how a connector loss comprised of all three alignment problems will change over the wavelength scan used for H_2S gas detection. The minute changes in losses shown in the figure are not normally noticed. This figure is included only to demonstrate that there are no nonlinear effects in connector coupling.

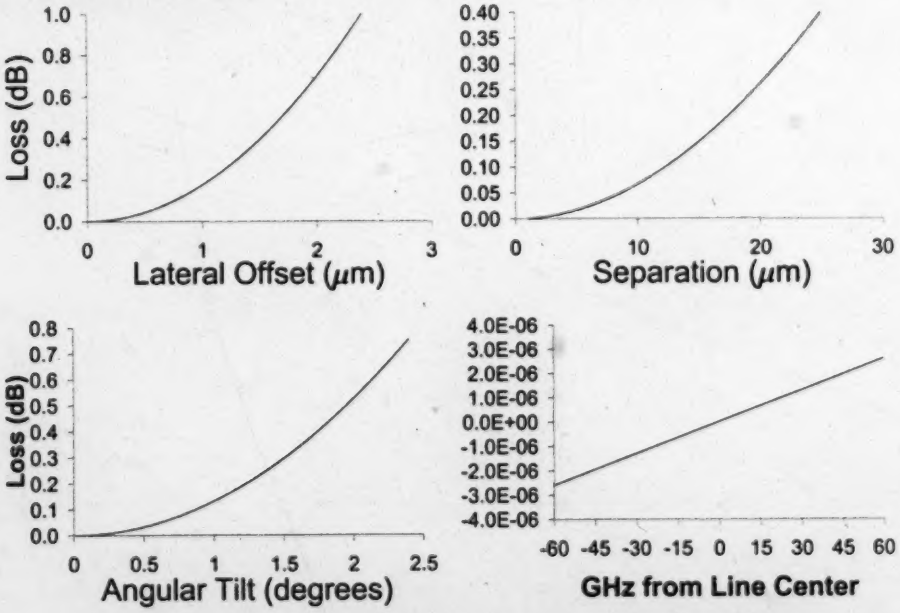

Figure 3.2: Loss Dependance on Connector Mismatch

Fiber to fiber coupling was accomplished in this project with already available bulkhead connectors. Two different styles of SingleMode fiber connectors were evaluated. The principal difference between the two types is the material used in the alignment sleeve. The material used in Methode connectors is Phosphorus Bronze while the Molex connector uses a Zirconia ceramic alignment sleeve. The results of evaluations conducted on each connector are included in Table 3. The use of index matching fluid between the interfaces will result in lower losses. A loss of 0.3 dB at a connector interface is considered average and acceptable.

Connector Style	*Loss Measured (dB)*
Methode: Phosphorus Bronze	- 0.3
Molex: Zirconia	- 0.5

Table 3

In a development system such as this, it was necessary to use connectors for ease of testing and experimental flexibility. In an engineered system that is to be installed, it is recommended that fiber be spliced together to minimize losses and backreflections.

3.2.2 Fiber Collimation

Once the light reaches the remote head, it must be launched onto the free space path over which we wish to detect gas. Proper collimation of the beam depends on a lens to compensate for how light is emitted from the fiber optics.

The emission characteristic of a fiber optic can vary a great deal depending on the type of index profile or fiber used. For MultiMode fibers, the distribution will depend on the amount of light in the various propagation modes, while for SingleMode fiber the intensity will be roughly gaussian. In this case the light will exit the end face of the fiber with a characteristic maximum launch angle. This angle defines the numerical aperture of the optical fiber and also determines at what angle incident light will be accepted into the fiber.

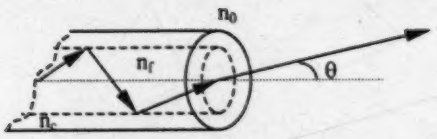

Figure 3.3: Fiber Emission Numerical Aperture

Noting Figure 3.3, we define the Numerical Aperture by $NA = \sqrt{\left(n_f^2 - n_c^2\right)} = n_0 \sin\theta_{max}$, where n_0 is the index of the medium the light is emitted into. Thus, the NA is different when launching into different media.

An experiment to profile the output of the SingleMode fiber used in this project yielded Figure 3.4. The data was taken 46.5 mm from the source fiber using a 0.2 mm^2 infrared detector detecting 1310 nm light emitted from a 9.3 μm fiber core. The line fit corresponds to a theoretical gaussian emission from a NA=0.13 fiber source.

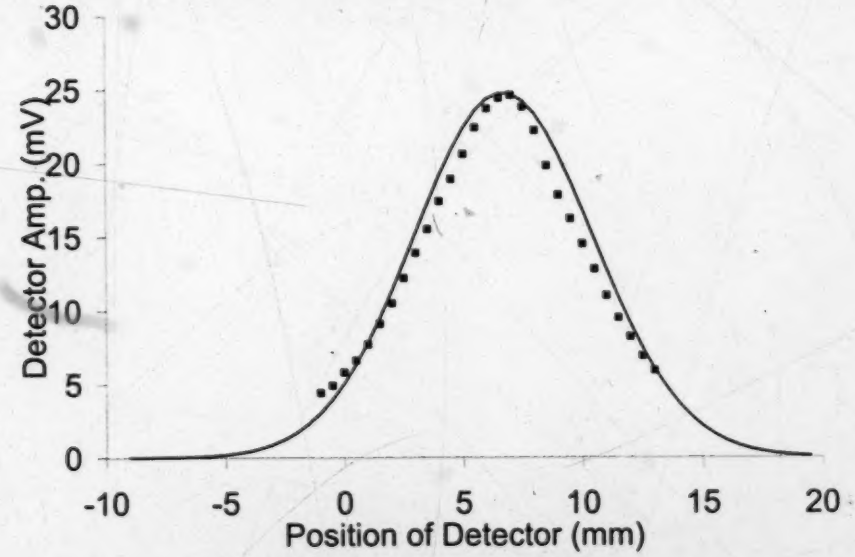

Figure 3.4: SingleMode Fiber Emission Characteristics

Collimation of the emitted probe light is necessary to precisely point the beam at the distant retro reflector [q.v. §4.4]. Considering the etalon problems described in §2.1.2, careful choice of the collimation optic is necessary. Two types of collimation lenses were tested in this

project. The diameter of a collimated beam determines the divergence of that beam. Therefore it is important to choose the largest launch beam diameter possible to minimize the beam divergence while keeping the etalon noise considerations in mind. The use of an Aspheric to collimate the beam at the remote head was the best choice. GRIN lenses, on the other hand, were more useful for the reference cell and optical test base described in §5.2. For this application, the economy and superior fiber coupling properties of GRINs prevailed.

I. Aspheric Lenses

Aspheric lenses are thin lenses which are fabricated out of molded plastic rather than glass. Classical glass lens grinding methods create optically imperfect spherical surfaces, which lead to aberration. However, the use of molds in the fabrication process allows for aspheric surfaces, the perfect lens shape to minimize spot size, to be easily implemented. Because of the manufacturing method, much smaller lens sizes which are more suitable for fiber optic products are also a possibility. Another advantage of the aspheric lens is the fact that the lens surface is curved which spreads the reflected light out over a large area, hence reducing backreflections much below 60 dB. This is important to reduce fiber etalon noise.

The aspheric that was chosen for evaluation was the AC210T, f = 11 mm lens available through ThorLabs Inc. This lens provides a good compromise between lens thickness, which is thinner than the regime where etalon noise is present, and launch beam spot size, which is larger than with GRIN lenses. The parameters outlining the quality of collimation for this lens are given in Table 4

Properties of the AC210T Aspheric Lens	
Launch Beam Diameter	2.2 mm
Half Angle Divergence	0.4 mrad
Focal Length	11 mm
Lens Thickness	2.35 mm

Table 4

This lens was used by ThorLabs Inc. and Oz Optics Inc. to develop collimation packages. The ThorLabs Inc. fiber collimation package,

F220FC-C, uses the lens in a factory pre-aligned module which is optimized for the 1050 nm – 1550 nm region. The H_2S absorption line is at 1578 nm and is therefore slightly out of the optimal region. However, the collimation is still better than the GRIN lens as the launch beam diameter is much larger. The Oz Optics HPUCO collimation package is a much more comprehensive and useful package but is also twice the price of the ThorLabs version. This collimation package relies on the user to optimize the position of the lens and fiber. This in itself is a very time consuming process, but superior collimation can, in principle, be obtained.

II. GRIN Lenses

The Gradient Index [GRIN] lens offers a simple alternative to the standard spherical lens. GRIN lenses are extremely economical, providing quality collimation in a small package. The focal length of these lenses can be altered by grinding them down to vary the length of the lens. Backreflections can be minimized by the use of antireflection coatings and angle cut end faces. These lenses have become the standard collimation method for fiber optic communication applications.

GRIN lenses are a cylindrical block of glass where the index of refraction varies with the radius. The parabolic index variation used causes all the impinging optical rays to be steered back towards the center of the lens. Figure 3.5 demonstrates the basic principle of GRIN lens fiber output collimation. The refractive index of the lens at a defined radius r is given by:

$$N(r) = N_0(1 - \frac{A}{2}r^2)$$

where N_0 is the index of refraction at the center of the cylindrical lens. The gradient constant A defines how drastically the refractive index changes with radius. The pitch of a GRIN lens is defined using: $P = \frac{\sqrt{A}Z}{2\pi}$ where Z is the length of the lens. The pitch defines the spatial frequency of the light ray trajectory in the cylindrical lens. By refering to figure 3.5, we see that a 0.25 pitch defines a lens that either completely focuses a collimated beam or collimates fiber output.

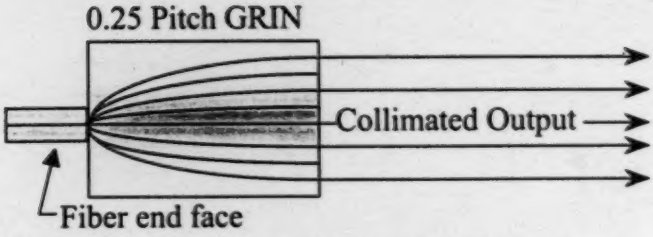

Figure 3.5: GRIN lens Collimation Example

A variety of lenses were used in the development of this project. One problem that arises is that the length, Z, of the GRIN lenses is normally in the realm of 5-10 mm, which is precisely the thickness of glass that will cause etalon noise to be imprinted on the signal. The amplitude of the etalon noise was minimized by using 8° angle cut lenses in addition to an anti-reflection coating on one end face. Table 5 describes the important parameters of the GRIN lens used for this project.

Properties of the GRIN GLW8580-1550 nm Lens	
Launch Beam Diameter	0.5 mm
Half Angle Divergence	2 mrad
Lens Length	4.8 mm

Table 5

3.2.3 Absorption

Attenuation of the light within the fiber via scattering and micro-bending losses is an extremely small contribution to overall losses. The development of low loss fiber was extremely important for the communications industry in their quest for long haul networks and therefore they developed low loss fiber optic. In the wavelength region where TDLS is possible, the losses in SingleMode fiber are only ~ 0.25 dB/km [41]. The use of connectors, which can have a loss of 0.5 dB/connector [41], is the more dominant fiber loss mechanism when it is considered that it is quite unlikely that the remote detector will be situated any further than 1 km away from the central system. However, if the fiber is strained, twisted or kinked in any way, the losses will become more pronounced. These flaws create small cracks in the glass fiber core, which will then scatter more light out of the core. It is also possible that these fiber flaws could exhibit wavelength dependent

absorption, which is precisely what TDLS detects. For this reason proper installation is important.

Installation should not exceed the minimum bending radius, the maximum tensile rating or the maximum vertical rise of the fiber used. Proper care should also be taken if the fibers are already connectorized because connectors are especially fragile and play an important role in the overall system loss [44].

3.2.4 Dispersion

The phenomenon where the velocity of propagation of an electromagnetic wave is wavelength dependent is commonly referred to as dispersion. The dispersion that any given fiber exhibits, can originate from a variety of sources. Chromatic dispersion occurs as a result of the variation of the index of refraction of glass with wavelength. Modal dispersion is another type of dispersion which occurs in MultiMode fiber and to a much lesser extent in SingleMode fiber. The propagation theory outlined in a number of texts [37-39,45], provides the basis for dispersion. In Multimode fiber, the difference in propagation velocity between the many modes is by far the most pronounced type of dispersion and severily limits the optical bandwidth of MultiMode fiber. Because of the bandwidth requirements of the TDLS technique, we were unable to use MultiMode fiber for probe light delivery.

Forced to use SingleMode fiber, it was still necessary to try to predict at what distance the fiber dispersion would begin to degrade system sensitivity. The effects of dispersion in SingleMode fiber are primarily a result of chromatic dispersion. The literature on the effects of chromatic dispersion on analog AM or FM communication systems is extremely scarce. However, the one analysis that was found predicted a maximum distortion of 60 dB between the first and second harmonic of a 100 MHz signal link after 100 km of standard SingleMode fiber [14]. It is therefore extremely unlikely that we should see any dispersion induced signal distortions with the remote heads situated less than 1 km from the central system.

3.3 Optical Splitter

Optical splitters use guided wave optics to manipulate light between different guiding structures. The basic physics that is used in all these instruments is the tunneling effect of the photon in confined optical structures. The electromagnetic wave, when confined in a guiding structure such as a fiber optic or waveguide, will have an exponentially decreasing field strength further away from the core of the structure. This evanescent wave can be used to couple some of the light out of the structure by positioning a material with a differing refractive index within this evanescent wave. In a wave guide this can be done by simply placing a prism on top of the guide and thereby coupling light out of the waveguide. The technique in fiber optics involves twisting two fibers together such that the evanescent wave from one fiber is present in the guiding structure of the other fiber. A small percentage of the light will then be coupled into the other fibers. Depending on how many fibers are used, the number of times the fibers are twisted together and the type of fiber used a wide variety of splitters can be created.

The important formulae and operating parameters for a 1 X 2 splitter are defined below. The quantities I1, I2, O1 and O2, shown in Figure 3.6, are the optical powers in each port defined in mW.

Coupling Ratio (%): $\left[\frac{O2}{O1+O2}\right]$

Coupling Loss (dB): $01\ \text{Port} = -10\ \text{Log}\left[\frac{01}{O1+O2}\right]$

$02\ \text{Port} = -10\ \text{Log}\left[\frac{02}{O1+O2}\right]$

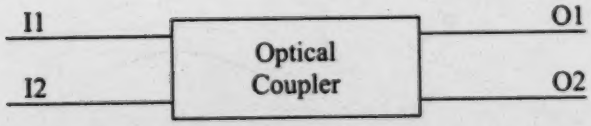

Figure 3.6: Optical Coupler Connector Diagram

Insertion Loss is defined as the sum of the coupling losses, the excess loss and any polarization dependent effects [46]. In addition to these losses, a connector loss of ~0.3 dB must be added at each fiber interface.

Splitters are a convenient method of splitting light onto a number of fibers such that the remote detection sites and the reference cell could be supplied with probe laser light. The path of the probe light is shown in Figure 3.7.

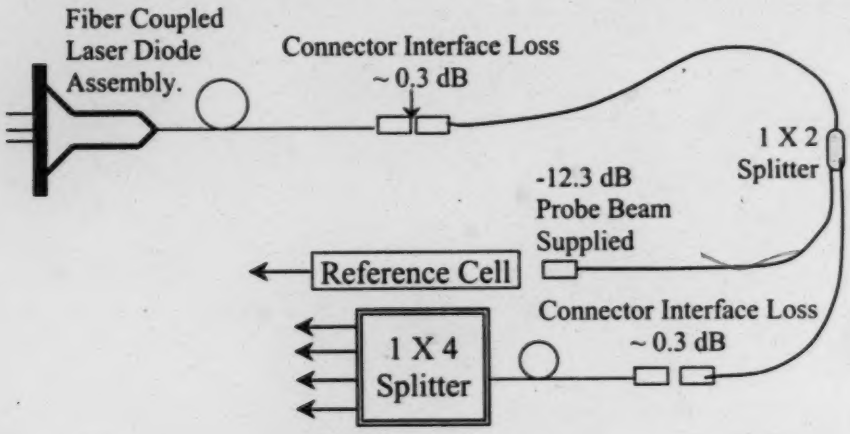

Figure 3.7: Fiber Optic Probe Beam Supply Network

To start, the light emitted by the Laser diode fiber passes to the first splitter. Here, ~ 1 % of the light is directed to the reference cell arm. The parameters defining this 1X2 splitter are included in Table 6

Reference Cell Supply Splitter Properties

Model:		Gould #50-10335-01-12561
Test Wavelength:		1553 nm
Coupling Ratio		1%
Loss from IN	Port O1:	0.07 dB
Port (I1) to →	Port O2:	22.47 dB

Table 6

Once the reference arm has been supplied with probe light, the remaining light is passed to a 1 X 4 splitter which splits the light into 4 equal parts. The manufacturer defined parameters for this splitter are included in Table 7.

Remote Head Supply Splitter Properties

Model:		FOCI C-TS 1X4 SingleMode Tree Coupler
Test Wavelength:		1310 nm
Coupling ratio:		25%
Loss from IN Port I1 to →	Port O1:	6.8 dB
	Port O2:	6.7 dB
	Port O3:	6.6 dB
	Port O4:	6.6 dB

Table 7

Noting the variation between remote head output intensities shown in the following table, it should be remembered that the manufacturer specified parameters are obtained using a different operating wavelength. While the 1X4 splitter does not split 1578 nm light equally onto its 4 outputs, there is still ample light to supply each head. The probe beam output intensities at all outputs are included in Table 8

Probe Beam Supply Intensities

Reference Cell	-12.3 dBm
Remote Head 1	1.3 dBm
Remote Head 2	3.5 dBm
Remote Head 3	2.3 dBm
Remote Head 4	-0.8 dBm

Table 8

Two tests are required to ascertain that the splitters are usable for TDLS gas detection systems. The first test is to show that they do not cause noise. This is demonstrated in Figure 3.8. This test was completed by acquiring a signal scan waveform both before and after a test splitter. The detected light intensity was equalized using the optical test base described in section 5.2.1. It is easily seen that the waveforms are not identical. This could not only be a result of the splitter but also from connector differences. The essential point is that the imprinted noise does not increase in size after a splitter. More analysis of the imprinted noise is included in §5.6.

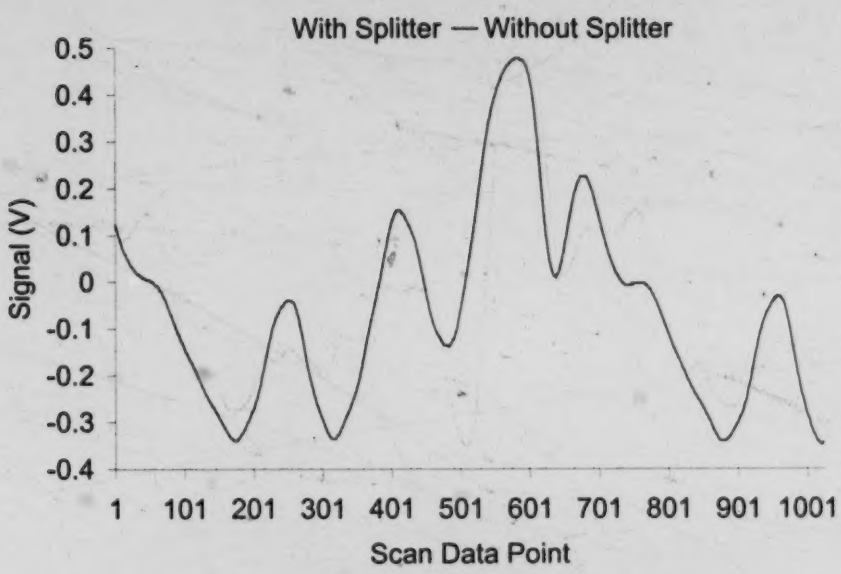

Figure 3.8: Demonstration of Splitter TDLS Transparency

The second test which is necessary is to verify that the gas signal is unaffected by the splitter. This test was performed in the same manner as with the TDLS transparency except that a reference cell was inserted in the optical test base.

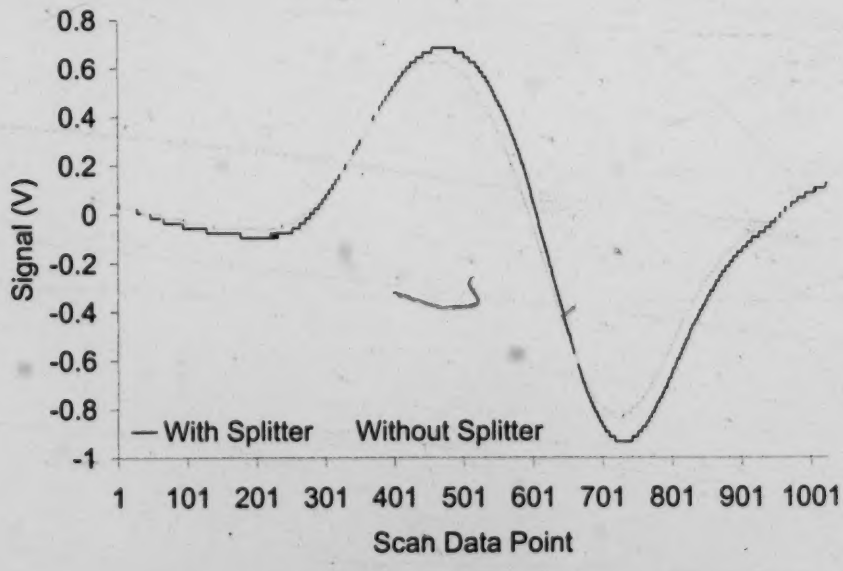

Figure 3.9: Effects of a Splitter on a Gas Signal

The light division and delivery methods involved directly splitting the probe light via two splitters. Another possibility entails using an optical switch to cycle the probe light output from head to head in a predefined order. The output from the laser is quite large and thus each head would receive excess light if this method were used. Optical switches are also extremely expensive in comparison with splitters.

4. Remote Head

Once the probe light has been split, it is delivered to the detection sites via SingleMode fiber. This chapter outlines the important components and design of the Remote Head that launches and receives the probing light along the path of interest. Figure 4.0 shows the remote detector head side view. The head is mounted on top of a tripod for experimental evaluations.

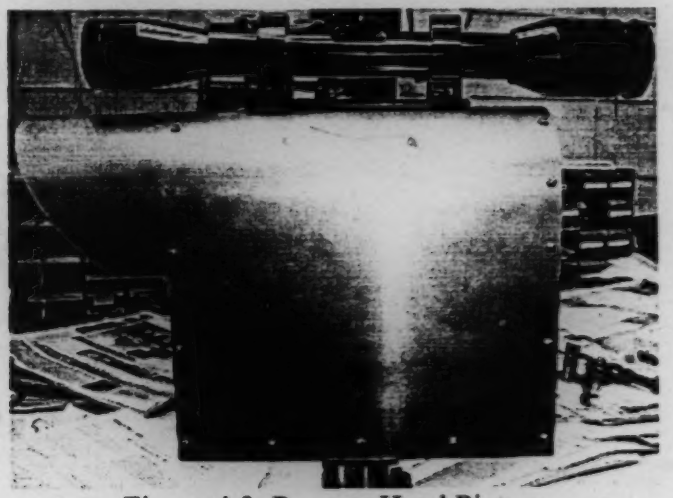

Figure 4.0: Remote Head Picture

At the beginning of the project, considerable effort was expended in researching the feasibility of developing an all-optical detection head. The approach in mind, involved collecting the probe laser light back into a SingleMode fiber optic. This method would have several key advantages. First, the remote heads could be placed extremely far from the central analysis system because of the low loss SingleMode fiber used. Secondly, no electricity would be supplied to the remote detection heads, allowing them to be placed in highly flammable environments. Unfortunately, the effects of atmospheric turbulence prohibited reliable coupling of the probe beam back into a SingleMode fiber.

The inability to avoid these inherent difficulties forced the development of a remote detection head that depends upon a +15 V DC power supply. The use of electricity means that these heads may not be placed in potentially explosive environments without significant explosion proofing being undertaken.

4.1 Design

As shown in Figure 4.0, the remote head is made of several machined aluminum pieces and a stainless steal cover. The completed head measures 20 cm long by 9 cm wide by 25 cm high. A Mylar window allows the light to enter and exit the instrument with minimal added noise. A glass window could not be used because of the possibility of etalon reflections creating noise. The instrument is protected from contaminants by using weather stripping between the cover and the remote head frame. A block diagram of inside the remote head is shown in Figure 4.1.

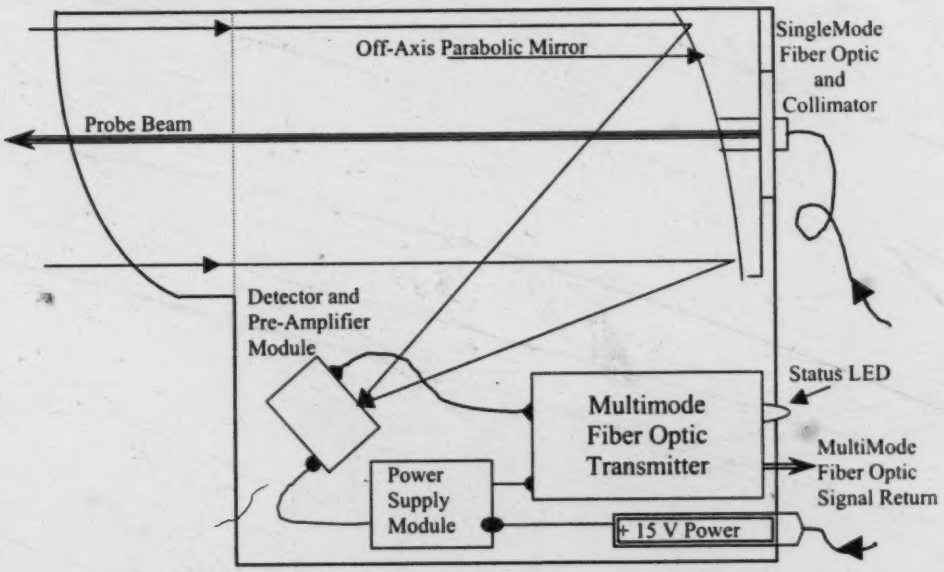

Figure 4.1: Remote Head Block Diagram

4.2 Alignment Procedure

Proper alignment of the remote head is crucial in order to detect light after a long optical path. For the remote head developed in this project, the light is launched on the optical axis of the instrument and aimed onto the probe path. The light is returned to the head by a retroreflector at the end of the path and then it is received by the

collection optic and focussed onto the detector element. A slight launch angle with respect to the optical axis will cause an oval focus in the wrong location. This will result in low light detection, making it important that the probe beam be launched properly.

The aspheric lens collimates the light as it exits the SingleMode fiber. The collimated beam is aimed using a crushed O-ring design, developed by Oz Optics [47]. This coupler is attached to the back of the remote head such that the beam is launched through the center of the parabolic mirror. The line-up procedure developed to point the beam onto the optical axis follows:

1. Couple visible laser light into launch fiber optic.
2. Place reflective tape ~2 metres from the remote head.
3. Observe the position of focal spot produced near the detector element.
4. Use adjustment screws on coupler to roughly align the outgoing beam so that it coincides with the optical axis of the collection optic. This is done by observing the focal spot and by adjusting the aiming such that the spot is closer to the detector element and is as round as possible.
5. Move the reflective tape a few metres further and readjust the coupler to better align the focal spot with the detector element.
6. Repeat above steps as many times as necessary until spot is entirely on detector and reflective tape is ~ 10 m away from the remote head.
7. Switch from visible light to infrared probe laser light.
8. Observe the Light Value reading on GasFinder system.
9. SLOWLY adjust coupler screws to optimize Light Value.
10. When the Light value has reached its optimal value, move reflective tape further away. Use of an infrared viewer card is necessary to observe the infrared beam.
11. Reiterate coupler adjustment to maximize Light Value at each successively further reflector distance.
12. Once the reflective tape is far enough that the Light Value is below 1000, replace it with the retroreflector.
13. Continue optimizing light level with further and further distances. Note that this becomes more difficult with larger distances since a minute adjustment may cause the beam to completely miss the retro-reflector.

This is a time consuming process that requires patience. Hasty adjustments often lead to losing the beam position. This inevitably leads to having to retrace steps already completed.

4.3 Beam Pointing

One of the difficulties in obtaining a gas measurement is aiming the invisible probe beam at the retroreflector. This problem relies on the fact that the optical path is normally > 100 m and the retroreflector is only 7 cm in diameter. We can then establish that the remote head must be pointed to within 0.02°, which is a very tight alignment tolerance.

Steps 12 and 13 of the alignment procedure require that after the optical axis has been aligned, the probe beam must be aimed at the retroreflector target. Because the probe beam is invisible, it must be replaced with visible light to determine where the collimated beam is situated. This is normally done by using a fiber coupled Helium Neon laser and connecting the visible light carrying fiber with the probe beam fiber. It is important to couple the visible light into the probe beam fiber at the central system as touching the fiber at the remote head collimator can destroy the alignment that has already been achieved. Once the probe beam has been situated, alignment of the riflescope that is mounted to the top of the remote head is possible. It should be noted that because the collimator is optimized for 1550 nm, the visible beam will not be perfectly collimated and will therefore have a spot that is much larger than with the infrared probe light. Once the riflescope has been adjusted such that the cross-hairs coincide with the center of the visible spot projected at a wall at least 25 m away, the probe beam carrying fiber is connected to the remote head once again. The remote head is now roughly aligned such that a small Light Value should be possible when the remote head is aimed at the retroreflector target at 50 m. Further optimization of the light value is now performed by adjusting the launch aiming and remote head pointing more precisely. Several iterations of riflescope adjustment at further and further distances allow a confident alignment of the riflescope cross-hairs and the invisible probe beam. The scope used is a 77-3900 Bushnell Buckhorn 4 X 32 mm wide angle riflescope. It should be noted that the riflescope is off-set from the optical axis of the head by several centimeters and therefore will not be properly aligned for short distances.

4.4 Retroreflector

This device is used for returning the optical probe beam to the remote head for detection. The retroreflector is made of three mirrors placed such that they form the inside corner of a cube. This simple geometry has the property that any light ray impinging on the retroreflector will be returned back onto itself after reflecting off each of the three mirrors.

The retroreflectors purchased for this project were Omni-Wave Hollow Retroreflectors manufactured by PLX Inc. Hollow retroreflectors were chosen because of the etalons created within standard glass retroreflectors. A 2.5 inch clear aperture provided for ample room considering the size of the beam outlined in section 4.7. For experimental testing of the system, the retroreflector was mounted to a tripod.

The accuracy of a retroreflector determines the maximum deviation from parallelism between the incoming and outgoing beams. High accuracy retroreflectors are expensive and therefore the much cheaper 5 arc second accuracy retroreflectors were used.

4.5 Collection Optic

The remote head uses an off-axis parabolic aluminum mirror with a gold coating to focus the light onto the detector pre-amplifier. This optic is easily imagined as a small circular cutout of a paraboloid. The paraboloid is the aspheric for focusing an incoming plane wave to the smallest spot possible. Since the detector must not obstruct the incoming beam an off-axis portion of the paraboloid was chosen such that the focus was off to one side of the incoming beam. The collection optic also has a small, ~ 5 mm hole in the center of the optic which is used to launch the probing optical beam onto the optical axis of the optic. The following figure and table demonstrate the properties of the optic.

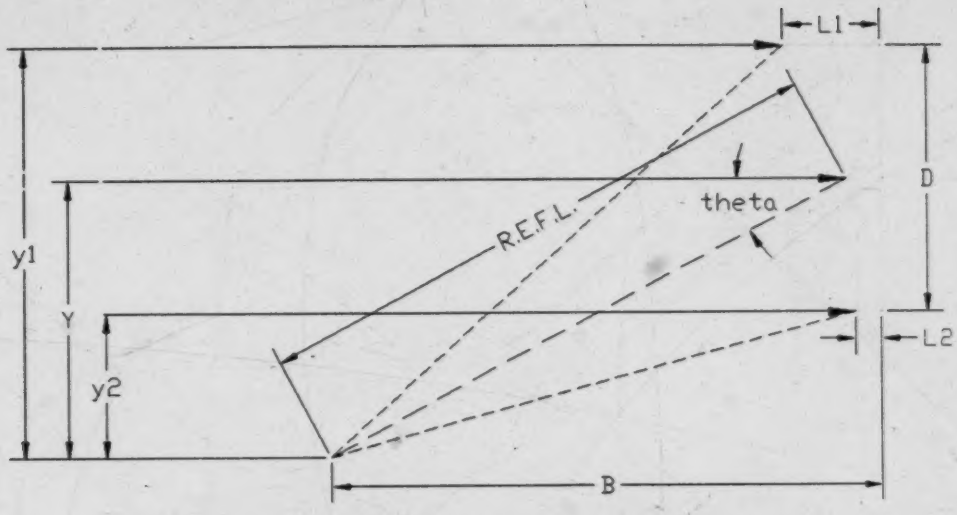

Figure 4.2: Off-Axis Parabolic Mirror Diagram

Off-Axis Parabolic Mirror Attributes

Y	Offset Axis	81.8 mm
B	Mount Distance	157 mm
D	Diameter	76.2 mm
θ	Angle of Focus	30°
R.E.F.L.	Reflected Effective Focal Length	163.3 mm
L1	Top Thickness	27.9 mm
L2	Bottom Thickness	7.6 mm

Table 9

The use of a 3 inch diameter optic provides ample light gathering capability which enables longer probe paths to be investigated. This optic has a small f-number of 1.1 which yields a very small focal spot. Diffraction analysis of the optic yields a predicted spot size of 2 μm assuming a perfectly plane incident wave. In fact, the machining process used to create the optic creates a slight diffraction grating on the optic leading to some light being lost in the resulting diffraction pattern.

Nonetheless, we expect the focal spot size is smaller than the 1 mm diameter photodiode.

4.6 Pre-Amplified Detector

The Boreal Laser GasFinder and the remote detection head designed in this project, use a Large-Area InGaAs PIN Photodiode to pick up the modulated optical signal. The reader is referred to any number of resources for the general properties of PIN Photodiodes [36-41,45]. The C30641 InGaAs PIN Photodiode manufactured by EG&G Optoelectronics Canada is ideal for this application because it is a linear device with its peak sensitivity corresponding to the wavelength we are using. The responsivity of an InGaAs PIN Photodiode in the 1550 nm region is ~ 1 mA/mW. These Photodiodes remain more than 99% linear when the detected optical power is less than 20 mW [48]. A reverse bias of 12 V is used to ensure that the photodiode is as sensitive as possible.

The pre-amplifier receiver uses this photodiode to provide a small current signal, which is then amplified by a transimpedance amplifier. The amplifier used is the Model 111 manufactured by Analog Modules Inc. This particular amplifier is low noise, i.e. 5 pA/$\sqrt{Hz}$, with a gain of 4.7 kV/A. It has a bandwidth of up to 100 MHz [49] and is mounted onto a PCB board.

A high-pass filter on the input of the transimpedance amplifier extinguishes the low frequency ramp oscillation, allowing the 10 MHz, 20 MHz and higher harmonic signal carriers to pass. Figure 4.3 demonstrates the performance of the pre-amplified detector for a variety of incident intensities.

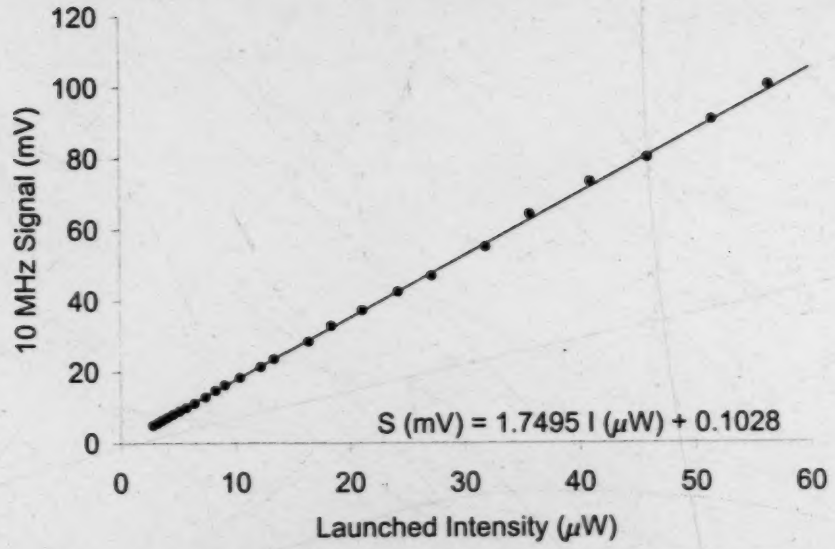

Figure 4.3: Signal Created by Pre-Amplified Detector vs. Light Intensity

4.7 Beam Propagation

The free space propagation of a gaussian laser beam is defined by the following formula [45]:

$$W(z) = W_0\sqrt{1+\left(\frac{z}{z_0}\right)^2} \quad \text{where } z_0 = \frac{\pi W_o^2}{\lambda}$$

W_o defines the half width of the focussed beam and z is the propagation path length. The probe beam wavelength is 1.578 μm and the launched beam waist radius is 1.1 mm for the Aspheric collimation lens used. Using this data, the following table for beam diameters was constructed to provide a feel for the beam at various propagation path lengths.

Beam Waist at various Propagation Path lengths					
Path Length	50 m	100 m	200 m	500 m	1 km
W(z)	2.2 cm	4.5 cm	9.1 cm	22.8 cm	45.6 cm

Table 10

4.8 Turbulence

An electromagnetic wave will propagate as described in §4.7 only if the atmosphere is a static, constant homogeneous medium. In free space propagation, it would be naive to assume that the index of refraction is constant over the entire probe beam path. In fact, the atmosphere is swirling about as a result of minor thermal variations present everywhere. This will surely effect the index of refraction in a multitude of indescribable ways. These effects are referred to as turbulence. A good review article on the calculation of turbulence effects by Ronald L. Fante explains these phenomena in detail [50].

Modeling the effects of turbulence on optical beams is an area of considerable depth and complexity. Optical beams suffer from beam spreading, intensity scintillations, beam pointing and other problems when they traverse regions of turbulent atmosphere. Quantifying these effects relies on precise determination of atmospheric parameters, such as temperature, wind velocity, cloudiness and others. Even when this data is known, the extremely intensive calculations required are only valid for a limited set of circumstances [51].

Because of these difficulties, models and experimentation on the turbulence problem were not investigated. The effects, however, are still present. Therefore, a brief discussion of the important aspects of turbulence in TDLS systems in included here.

The theory of turbulence assumes the existence of eddies within the air in which the beam propagates. A wide range of eddy sizes are possible. Each eddy can, in principle, have a different optical index as a result of density differences. Depending on the relative size between the coherence length of the beam and the size of the eddies, the beam will either be deflected in a slightly different direction or the phase front of the beam will be delayed in certain areas. As the beam travels through a large number of these stochastic refractive index disturbances, the beam quality will be degraded.

The most important effect of turbulence on the gas detection technique used in this project are beam spreading and scintillation. As turbulence increases the beam will spread at a faster rate than is predicted using standard gaussian beam analysis. This will lead to lower light

detection levels since less light will be collected by both the retroreflector array and the collection optic. Intensity fluctuations on the detected light level will occur because of phase distortions imprinted on the beam constructively and destructively interfering. However, aperture averaging will decrease the intensity of these scintillations by the use of as large a collection optic as possible [50].

Scintillation effects can degrade sensitivity by causing a variation in light detected over the scan frequency. For this to occur, the scintillation must manifest itself with a time scale that is shorter than that of a scan. This can and will occur but the scintillation is a random process and therefore will be averaged out over the many successive scans averaged to provide a signal to be analyzed.

4.9 MultiMode Fiber Optic Link

After the launched beam has propagated over the path to be probed and the pre-amplified detector has converted the light into an electrical signal, it must be returned to the central system for analysis. The relative signal amplitude difference between the 10 and 20 MHz oscillations produced by the electro-optic conversion must remain constant if we are to retain the gas concentration calibration. It is therefore necessary that the link between the remote detector heads and the central processing unit have a minimum, distortion free bandwidth of 25 MHz without distortion.

For this project the choice was made to use already developed fiber optic link systems for cable television. The choice to use a fiber optic link is judicious for several reasons. A fiber optic based link maximizes the distance over which the signal can be transmitted. The signal is transparent to electromagnetic interference and the associated link electronics are simple. For these among other reasons, the high definition television [HDTV], closed circuit television camera, and cable television industries have developed these links for their applications. Luckily, the bandwidth requirements for this project are roughly the same as a HDTV Video transmission link. In the interests of cost reduction and engineering simplicity, this type of link was purchased as the signal return method between the remote detection sites and the central processing computer.

The Fiber Options Series 175B, RGB Wideband Video Transmission System satisfied all the link requirements and was relatively inexpensive. The link consists of a transmitter, receiver and MultiMode fiber optic. Both modules require a 12-16 VDC, 200 mA power supply and are designed for 75 Ω impedance, RGB signals. The link can withstand a loss of 13 dB on 62.5 μm (Standard) MultiMode fiber without signal degradation. The system uses an 850 nm source and Automatic Gain Control [AGC] to compensate for the losses in the link [52]. Through testing, it was established that the link functioned with minimal noise for the domain of input signals ranging from 250 mV to 1.1 V at 10 MHz and 20 MHz. Figure A.1 in Appendix A demonstrates the fundamental operating characteristics of this link.

As shown earlier in §4.6, the pre-amplified detector supplies a signals in the realm of 10-120 mV. The Fiber Options link is manufactured to transmit standard video signals at ~1 V_{pp}, and therefore necessary to include a ~10 dB gain stage before the transmitter and then to attenuate the signal after the receiver. Details of the attenuation included in the analog switch design are included in §5.1.1.

The amplifier used to boost the signal so that it matches the characteristics of an RGB Video signal is a ZFL-500 Mini-Circuits amplifier. This amplifier exhibits a constant gain over the frequency range of 50 kHz to 500 MHz and therefore has plenty of bandwidth for this application. Unfortunately, the gain of this amp is 20 dB. It was therefore necessary to include a 111 Ohm resistor between the amp and the photodiode pre-amplifier to reduce the input signal such that the amplifier is not saturated. The input impedance of the link transmitter was modified from the factory value of 75 Ohm such that it agreed with the input impedance of the 50 Ohm output impedance of the ZFL-500 amplifier. The performance of the link with the amplifier added before the input to the transmitter is plotted in Figure A.2 in Appendix A.

The performance of the entire link is effectively transparent. As shown in Figure 3.0, the L.V. received through the reference arm or through the remote head arm is equal for a given amount of light hitting the detector. Figure 4.4 demonstrates that the perceived gas level for a given sample of 8000 PPMM, is roughly constant no matter how much light is detected. This shows that the relative amplitudes between the constituent signal harmonics have been preserved by the remote head

signal link. This test proves that the remote head gas sensitivity has been maintained.

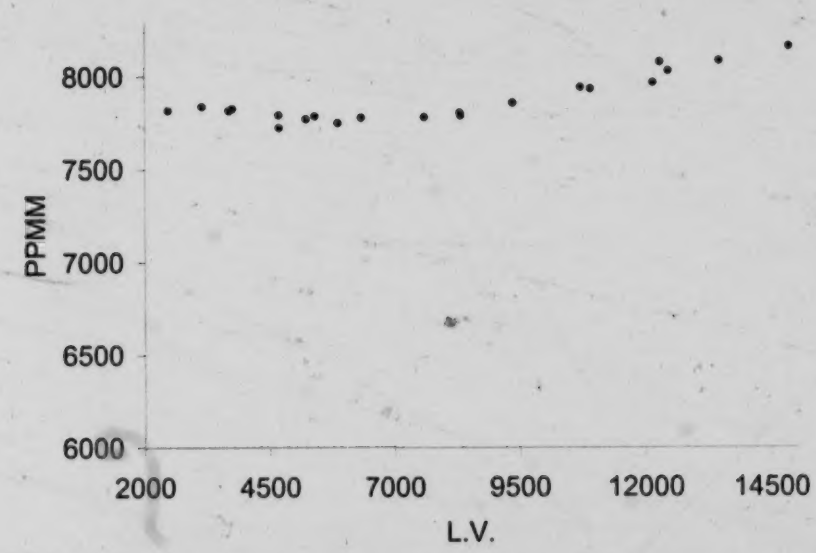

Figure 4.4: Light Intensity Test of Gas Concentration Stability

5. Signal Processing

The last step in determining the gas concentration detected lies in analyzing the signals returned from the remote heads. The analog switch described in §5.1.1 selects which signal will be passed on to the receiver board. The Boreal Laser Receiver board, described in §5.1.2, analyzes the modulation harmonics to provide a signal sweep for each scan of the laser diode. This signal sweep must then be processed to determine the gas concentration.

Real time processing of the signal scans demands considerable processing capabilities. As shown in Figure 1, the control computer maintains the laser diode tuning to the absorption profile and directs the analog switch to select which signal is to be analyzed. It must also convert the analog signals originating from the receiver board into digital signals via an A/D process and then average these signals. It must then calculate the gas concentration seen by comparing the averaged waveform with a previously stored reference signal.

The GasFinder computer that was integrated into the structure of this system was not designed as a multiple path detection system. Unfortunately, the control computer and the methods used were not upgraded and therefore real-time testing of the system was limited. It is therefore the goal of this chapter to explore possible additions to the computer software. The processing that was capable with the on-board computer system is demonstrated and described in §5.3. Section 5.4 explores some possible ways that the software for the system could be improved. Evaluation of new processing methods was completed using an off-line computer to perform the required computations and an oscilloscope to digitize the analog waveforms.

5.1 Analysis Electronics

The analysis electronics consist of the analog switch and the receiver board. These components select the signal to be analyzed and then converts the signal into a usable form for the computer Analog to Digital converters.

5.1.1 Analog Switch

As was shown in Figure 1.0, the system control computer, described further in §5.3, controls the analog switch. The software for the control computer was written for a single path gas detector and therefore only directs the switch to look at either the reference cell signal or the probe beam signal. The on-line computer periodically updates its reference waveform by supplying a logic signal of +5 V to the switch. This allows the computer to compare the waveform to a calibration waveform ensuring that the laser is properly tuned. Any adjustments in the operating conditions can then be made.

The analog switch, designed by Ben Bathgate for this project, allows for the same software to be used to monitor 3 paths. This was done by returning to consecutively different remote path signals after each reference cell check. Figure 5.0 demonstrates the switches principle of operation.

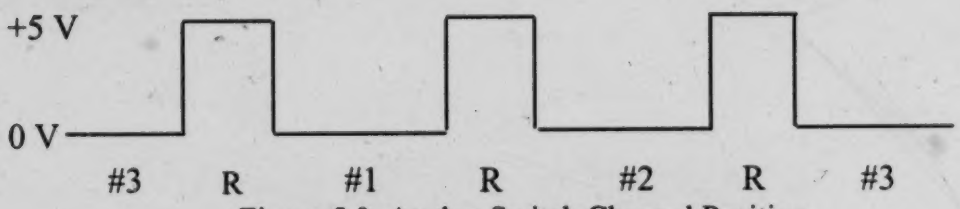

Figure 5.0: Analog Switch Channel Position

It is recalled that the signals that originate from the remote detection sites were amplified in order to be transmitted by the Multimode Fiber Optic links. Therefore, the inputs for the remote detection sites include signal attenuation and have a 75 Ω input impedance. The switch is based on TEMIC Semiconductors DG641 Wideband Switch with a Microcontroller to control the various inputs. The reference cell signal originates from the Pre-amplified detector, and therefore suffers minimal attenuation and is designed for a 50 Ω output impedance. The specifications for the Analog Switch are included in the following table.

Analog Switch Specifications	
Average cross-talk between channels:	25 dB
Reference signal attenuation:	0.76 dB
Remote signal input attenuation:	7.76 dB
Output impedance:	50 Ohm

Table 11

5.1.2 Boreal Laser Inc. Receiver

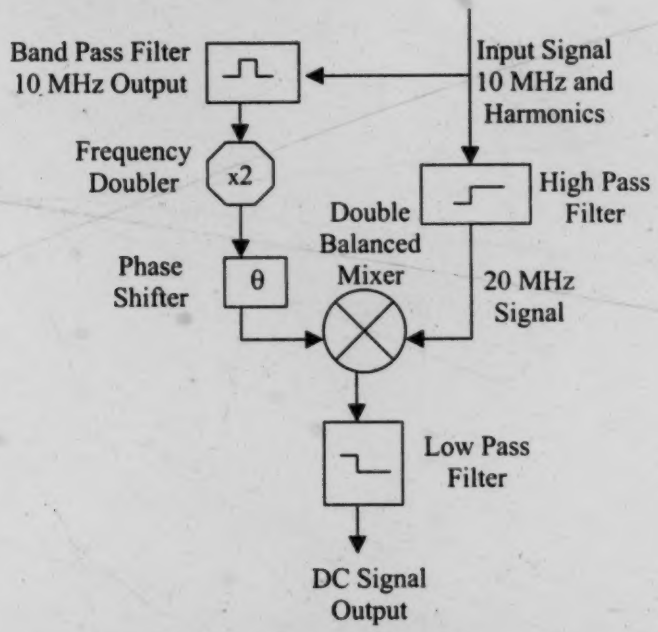

Figure 5.1: Receiver Block Diagram

Figure 5.1 demonstrates, in block diagram form, how the Boreal Laser Receiver analyzes the input signal. As the laser diode wavelength sweeps over the absorption profile, the DC voltage output created by the receiver traces out the signal which is then analyzed by the computer. This signal is produced by splitting the input signal into two arms and then mixing them with a double balanced mixer. The first arm signal passes through a high pass filter which only allows the 20 MHz signal to pass. The second arm filters out all frequencies except the 10 MHz component using a bandpass filter. The 10 MHz signal is then frequency doubled and a phase adjustment made before it is mixed with the original 20 MHz signal component. The output of the mixer then passes through

a low pass filter to eliminate the 40 MHz wave in favor of the DC signal sweep which is then fed to the Analog to Digital converter on the computer board. The phase shifter on the second arm must be set such that the absorption signal is at a maximum. This can be done with a quick turn of the phase adjustment while a test reference gas signal is being analyzed. Figure A.3, in Appendix A, is a plot of the various reference cell waveforms obtained for the entire range of possible phase shifts. This plot is included to demonstrate how the system sensitivity can be compromised by an inaccurate phase shift setting.

The receiver board also measures the raw signal strength. The magnitude of the 10 MHz input signal is then displayed on the front panel in the form of Light Value units (q.v. §3.1) The following figure shows the relation between an input 10 MHz signal and the Light Value units shown by the receiver board.

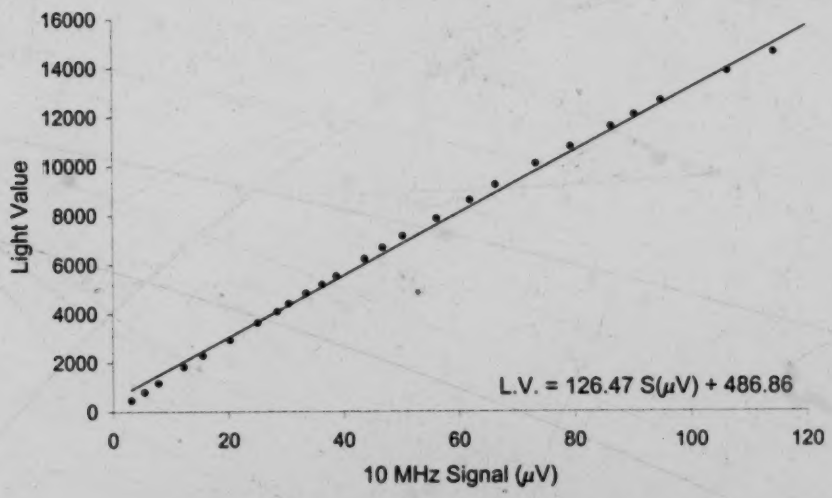

Figure 5.2: Receiver Board Signal Calibration

Another important aspect of the Boreal Laser Receiver board is its capability to gain switch. When the scan signal voltage rises out of the possible A/D converter range, the computer then instructs the receiver board to gain switch. The receiver board then attenuates the output signal by any of four possible gain multiplication factors, i.e. 1 X, 4 X,

8X and 32 X. The relevant factor is then used by the computer in its calculations to compensate for the gain switching.

5.2 Reference Cell

The ratiometric gas concentration calculation requires a reference gas waveform. For this project a small 8 mm diameter by 5.5 cm long glass cylinder was prepared containing a small amount of H_2S and the balance nitrogen, N_2, at 1 atmosphere. The ends of the cell were cut at 56°, the Brewster angle, to minimize reflections. The H_2S concentration within the cell after fabrication was not accurately known as a result of the gas handling practices used.

The standard to determine the gas concentration of the fabricated reference cell was a reference cell prepared by Boreal Laser Inc. which has a concentration of 8000 PPMM. Using this cell for comparison, the fabricated reference cell was found to have a concentration of 3760 PPMM. These two cells were used to verify the signals obtained by the gas detection system. The signals provided by these reference gas samples allowed the complete calibration of the system.

5.2.1 Optical Test Base

Because of the toxicity of H_2S, it is not an option to release the gas into the optical probe path for testing purposes. It was therefore necessary to develop an alternative method of introducing a test gas into the probe beam path. For this reason the optical test base was developed to provide a short section of free space probe beam in which a reference test cell could be inserted. This simple experimental apparatus proved to be extremely useful both as a calibration method and as a variable attenuator.

The test base consists of two fiber couplers and the support apparatus. The first fiber coupler collimates the probe light as it exits the SingleMode fiber and points the beam at the second coupler. This coupler collects the free space beam back into another SingleMode fiber optic. The GRIN lens described in §3.2.2.II was used as both the collimation and focussing optic.

The optical properties of the test base are that the launch beam is approximatly 0.5 mm in diameter. The distance between couplers is 10 cm and the loss associated with the entire test base is at least 1.5 dB. However, by slightly adjusting one collimation coupler, less probe light is coupled into the exit fiber and it was therefore possible to determine system parameters at all possible light levels.

5.3 On-line Processing

The Boreal Laser GasFinder that was integrated into the structure of this instrument included a computer analysis board. This board, the Freedom 16 v2.10 manufactured by Intec Automation Inc [53], performed all of the On-line data analysis and calculations described in this section. These algorithms were developed by Boreal Laser Inc. engineers. The data manipulation and analysis have a variety of parameters that can be adjusted to increase the sensitivity of the instrument in certain situations. Figure 5.3, portrays the various averaging and data manipulation techniques that can be manipulated from the GasFinder front panel.

The user interface is through a four button controller and small LCD display as indicated at the base of the Primary GasFinder Menu Layout [Figure 5.3]. Navigation of the various menus and adjustments is accomplished using the arrow keys, while the ENT key is used to enter a sub-menu or to change to adjustment mode. The ESC key is used to exit all menus or adjustment mode back to normal system operation. A more detailed discussion of the menu structure of the GasFinder software is included in the GasFinder 2.0 Operation Manual [54].

During normal operation the display menu shows the gas concentration reading, and the confidence factor, r^2. The gas concentration is displayed in either PPMM [Parts Per Million • Meters] or PPM [Parts Per Million]. The PPMM reading represents the total gas absorption signal over the optical path being probed while the PPM reading is the AVERAGE gas concentration over the entire optical path. The confidence factor, r^2, varies between 1 and 99 where 99 denotes optimal confidence. The coefficient of linear correlation, as the confidence factor is normally called, is a measure of the quality of linear fit obtained in the ratiometric calculations.

5.3.1 Standard On-line Processing

To begin, a brief review of the signals created by the gas detection technique will provide a solid base from which to understand the signal processing that must be performed by the Freedom 16 on-board computer. First, the modulation on the input into the laser diode comprises of the ramp, which sweeps the laser wavelength over the absorption profile, and the 10 MHz oscillation which is distorted by the gas absorption. The detector picks up the 10 MHz oscillation and it's associated harmonics and cuts out the ramp signal. The 10 MHz oscillation is manipulated by the receiver such that the gas signal outlined in Figure 2.1 is repeated with the same frequency as the ramp, i.e. 354 Hz.

The A/D section of the computer board converts the analog signal from the receiver into the easily processed digital domain. The digital information is synchronized with the ramp signal such that successive signal scans can be averaged to improve signal to noise ratio. The averaged signals are then compared to the reference waveform to determine the gas concentration reading.

In normal operation, the computer samples the waveform at 64 points per scan. The first 15 data points are discarded to compensate for the phase noise peak that is described in section 5.5. The acquired waveforms are averaged over N scans as is the reference cell waveforms. These two scan waveforms are then compared using the ratiometric technique described in section 2.1.1. The detected gas concentration, the coefficient of linear correlation and various other parameters are then posted to the RS-232 communication port on the back of the instrument to be logged. This information is also available in the various menus outlined in Figure 5.3.

Primary GasFinder Menu Layout

Figure 5.3

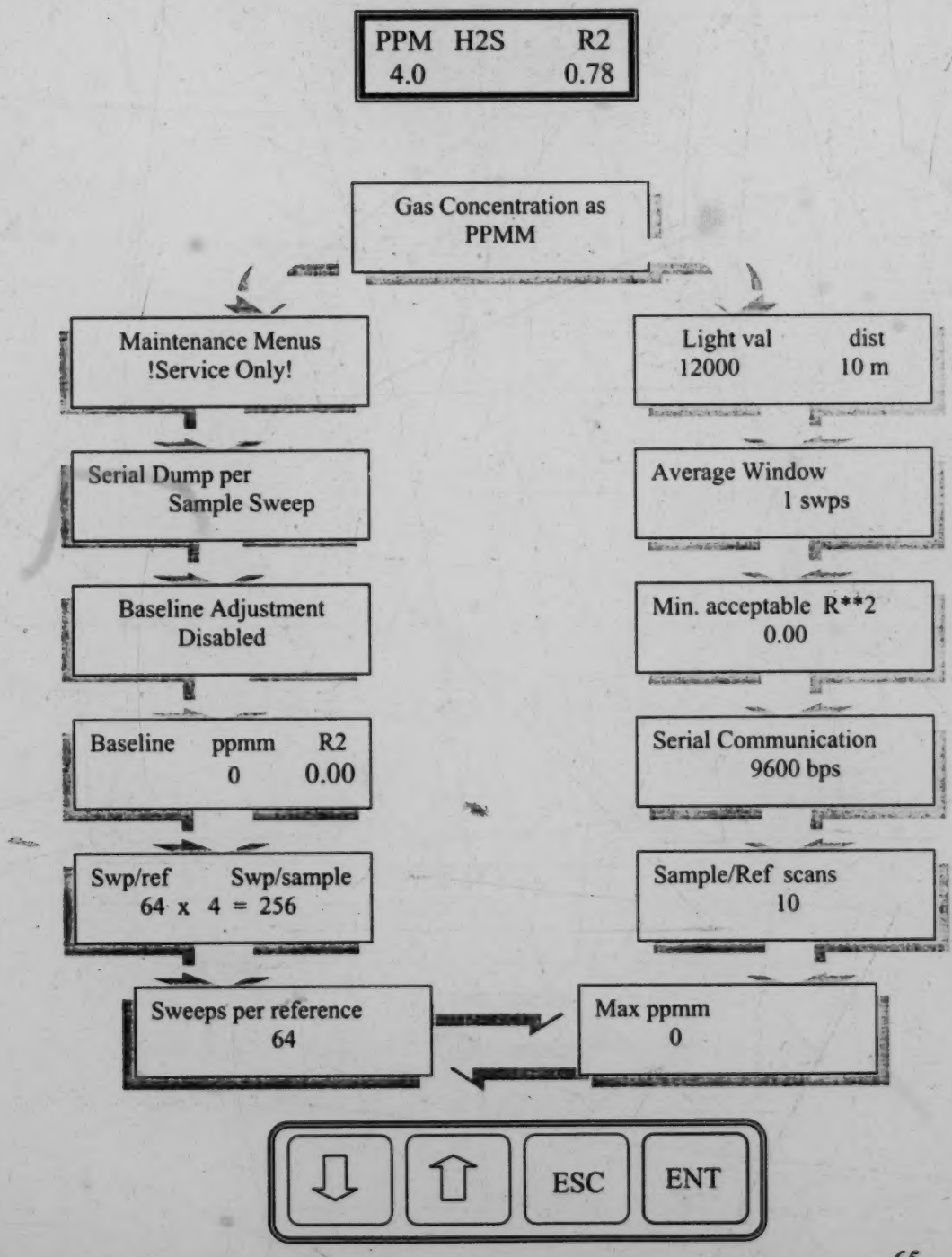

5.3.2 On-line Background Subtraction

The GasFinder system was also programmed to subtract a previously stored background waveform from the acquired signal in order to minimize the effects of spurious gas lines and other signal corruption. The stored background signal is manually acquired by entering the maintenance sub-menu of the GasFinder software. Once the background had been stored in memory, the computer then subtracts the value of the background signal from each corresponding sample waveform value and then adds a constant to prevent the possibility of system errors generated by negative numbers. Once the background has been subtracted from the acquired waveform, the subtracted signal passes to the ratiometric gas concentration calculations that were discussed before.

5.4 Standard Off-line Processing

There are both advantages and problems with the off-line data taking process. The use of an oscilloscope allows more samples to be taken from a selectable section of the scan waveform. A computer is also capable of more powerful processing of this acquired data then the on-line computer board. However, one major difficulty of the off-line processing technique was the inability to control the on-line computer and the associated receiver and transmitter electronics. The results of these difficulties are discussed in §5.6.2.

In order for the computer to be used to process the data, an oscilloscope, a Tektronix 2440, was used to acquire the receiver signals from the instrument. The oscilloscope used the system timing clock signal as the trigger of the analog signal scans produced by the receiver board. This allowed a window from each scan to be selected using the trigger timing. This window could then be continually averaged for SNR improvement. When instructed via the GPIB [General Purpose Interface Bus] interface, the oscilloscope would transmit the 1024 averaged data points of the desired waveform section.

All of the off-line data acquisition and processing algorithms were developed using the LabVIEW G programming language. These programs were run on a Pentium MMX 200 MHz computer.

5.4.1 Off-line Background Subtraction

The use of a computer in the data analysis allowed for a library of acquired signal scans to be retained as possible background waveforms. This allowed a more complete evaluation of the background subtraction technique.

The coefficient of linear correlation between the perspective background waveform and the acquired reference signal allowed the computer to reject a waveform from use as a background by comparing it to a user defined upper limit, *R*. If the coefficient of linear correlation for a given waveform was above this set point, *R*, the computer then rejected the waveform because of a possible gas presence in the signal. The computer would then look back in time to evaluate the previously acquired waveforms for a more suitable background waveform.

The other user defined parameter is the "waveform acquisition wait index", *N*. This feature delays the update of the background array until after *N* acquisitions have taken place. It will be shown in §5.6, that the averaged scan waveforms are reasonably stable over a period of time. The wait index is a method of monitoring any perceived gas concentration changes over time. This is to say that the calculated PPMM reading will reflect all changes in the waveform during the time since the background was refreshed. The wait index determines the length of time over which we wish to monitor waveform and hence gas concentration changes.

5.5 Signal Distortions

Understanding the noise characteristics of this system was among one of the most difficult hurdles to be overcome in the development of a reliable fiber based gas detection system. A variety of hypotheses and methods are presented in this section to explain and hopefully minimize the noise presence in the signal. As an aside, many hours were spent experimenting with system parameters in the hopes of both understanding how the noise came about, and how best to minimize the effect the noise had on system performance. The conclusions and results

of these hands-on experiences are detailed here and throughout the following chapter on results.

A brief description of what is meant by the term noise is necessary. If there is no gas present in the probe beam path, we expect that the scan signal waveform will be a flat line. Any variations from a flat line, except for gas signals, are considered here as noise. This noise could correspond to anything from wavelength dependent attenuation changes to harmonic distortions during the electrical signal manipulation.

It should be noted, however, that a wide variety of other noise types exist in the system. The fundamental quantum limited light detection process produces shot noise, while resistors and other electronics exhibit thermal noise. These noise sources result in up to 1 V_{pp} of variation between consecutive acquired signal waveforms. These deviations were averaged together to obtain an average signal scan waveform. It is this averaged waveform that is normally referred to as the scan waveform. A point of consideration is that as more waveforms are averaged together, the instrument will exhibit a longer response time This method of noise reduction results in a trade off between gas detection response time and an accurate representation of the absorption profile detected.

The operational settings of the laser transmitter board (q.v. §2.3) are crucial for optimal system performance. When the transmitter settings are being set it is important to observe the signal with and without the gas cell present. The systems primary goal is in the reliable, sensitive detection of a particular gas absorption profile. Therefore the set-up should be tweaked to provide the largest possible signal for a given test gas.

By switching between the reference signal and the raw probe beam signals, it is possible to set the transmitter such that the observed probe beam signal noise is at a minimum in the region of the H_2S signal. The various parameters which influence the baseline noise characteristics are the laser bias point, the RF modulation depth, the laser diode temperature set point, the balance coil on the transmitter board and the phase adjust on the receiver board. One method of minimizing baseline signal noise is to decrease the temperature set point, thus causing the operation wavelength to change, and compensating the wavelength change by

raising or lowering the injection current bias. At a new injection current bias, the laser diode could exhibit less second harmonic distortions and hence less noise.

The most obvious signal distortions are the large peaks obtained at the beginning and end of the laser scans. Figure 5.5 provides an example of this type of noisy waveform. Ramp beginning and ending distortions and receiver PLL instability are two of the possible sources of the phase noise. While it is likely that this distortion could be eliminated by rooting out the source of the problem, the time was not taken to examine the issue closely. It is, however, quite simple to side-step the problem. Figure 5.5 demonstrates that the phase noise peaks (marked by arrows) do not appear in the same section of the scan as the gas signal.

The phase noise peaks can, therefore, be cut out of the waveform used for the ratiometric calculations. The on-line computer does this by skipping the first few acquired points of the scan. The number of points skipped is set in the maintenance menu of the GasFinder software. For off-line processing, the phase noise peaks were not a problem as only a portion of the scan is acquired. Therefore, the selected window was centered around the reference waveform, excluding the phase noise peaks.

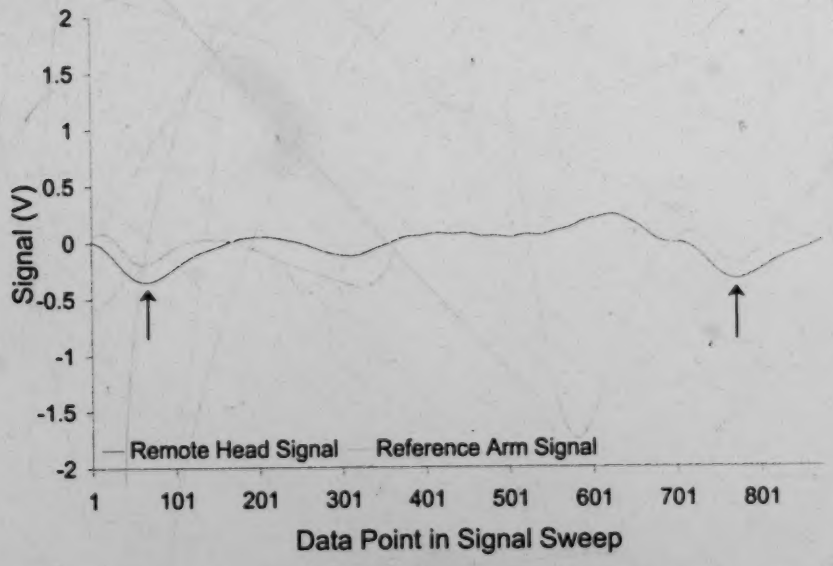

Figure 5.5: Demonstration of Phase Noise Peaks

The data shown in Figure 5.5 juxtaposes the probe signal waveform and the reference waveform to show that the phase noise peaks are not in the same region as the gas signal. This, however, obscures the fact that the phase noise peak is the largest noise contribution in the probe signal scans. The other noises present in the signal scans are not visible because of the range of signal values plotted. Figure 5.6 shows an example of the unprocessed noise received by the detection system. The arrows on this plot show examples of spurious noise ripples that are in the domain of the gas signal and will cause errors in the perceived gas concentration.

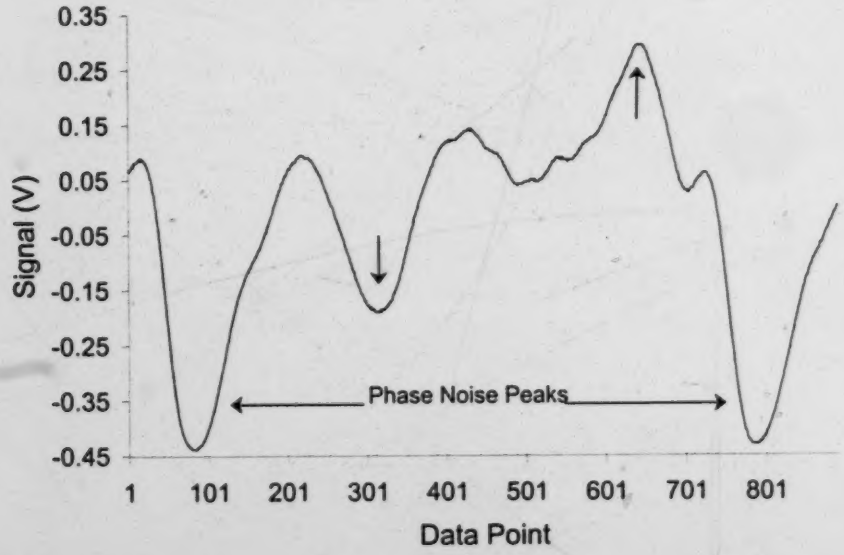

Figure 5.6: Unprocessed Waveform to Demonstrate Phase Noise

Figure 5.6 demonstrates that the phase noise peaks are the largest source of noise, but it is also important to note that the form of the acquired waveform will depend a great deal upon the phase shifter setting on the receiver board. In Appendix A, Figure A.4 demonstrates the range of possible signal waveforms for the entire range of possible phase shifter settings. Figure A.4 shows that the center of the signal scan is relatively unaffected as a result of phase shifter settings. We, therefore, conclude that the phase shift setting should be chosen such that the reference signal is maximized. The phase noise peaks associated with this phase shift setting can be excluded from the data acquired.

The existence of etalon like noise imprinted on the probe beam has been seen in Figure 5.6. This noise is largely unavoidable but can vary a great deal in size. Extensive experimentation has shown that if the imprinted noise is causing significant problems, one must simply change the alignment of the remote head, clean fiber optic connections, or move the fiber optics to change the noise profile to a less intrusive, less gas-like shape. Changing the transmitter settings is also an option. However, experience has shown that through system maintenance, cleanliness and trial and error, the imprinted noise can be decreased to respectable levels of less than 300 mV_{pp}.

The stability of the imprinted signal distortions is extremely important for reliable gas detection readings. If the imprinted noise is stable, we have the possibility of subtracting off this background noise. However, if it is not stable we are left with a gas detector with a large error in perceived gas concentrations as with each new background noise signal comes a new PPMM reading. Figure 5.7 demonstrates the stability of the acquired signals over a period of 50 minutes.

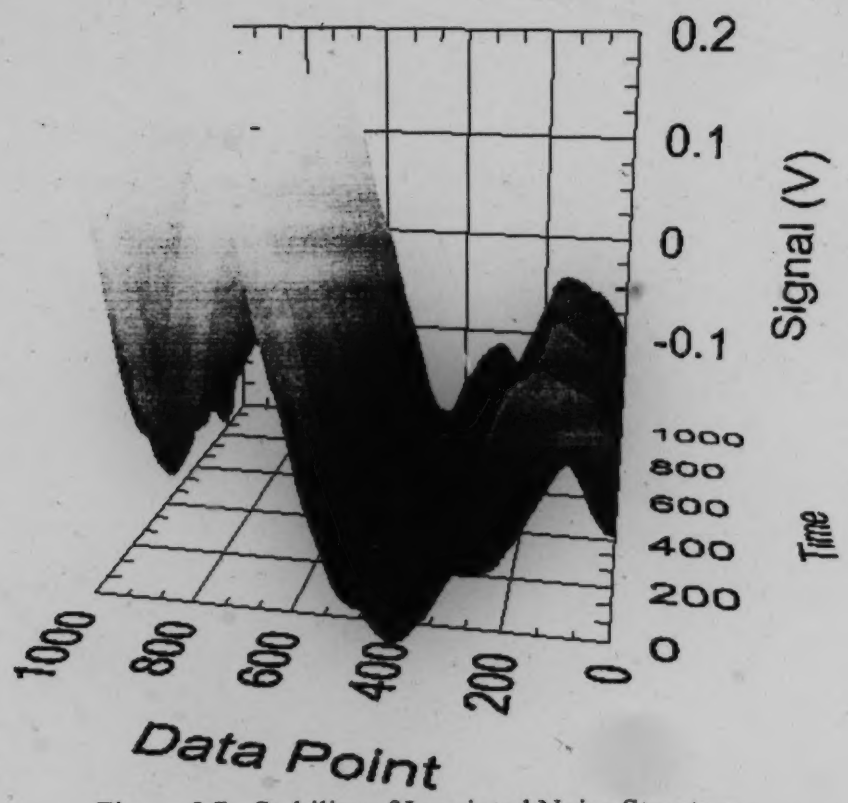

Figure 5.7: Stability of Imprinted Noise Structure

This figure clearly demonstrates that we do not expect the background signal to vary a great deal over time. Some small variations are due to the slight thermal variations of the laser diode, which cause wavelength drift. This results in small lateral shifts in the background noise structure. The small variations in the signal voltage at a given point indicate small changes in absorption. The important point, however, is that the noise structure is for the most part stable over short intervals of time. This allows the use of background subtraction as a method of eliminating the imprinted signal noise. Further discussion of the stability of the background structure lies in the analysis of the results of the background subtraction methods, §5.7.4.

The structure of the unprocessed waveforms shown in Figure 5.6 and Figure 5.7 are quite different in form. This could be as result of changes in where the beam hits the retroreflector, in the way the probe

beam carrying fiber was laid, or how much light was received. It is therefore necessary to set-up the remote head and all the fiber optics entirely before one can consider the background stable, and it is only considered stable until something is changed or manipulated.

5.6 Results

This section demonstrates and discusses the signals and results obtained while testing the instrument. The on-line processing results were obtained using the standard ratiometric processing, which the on-board computer is capable of performing. The off-line processing section presents the results of investigations obtained using powerful, versatile data processing techniques.

5.6.1 Standard On-line Processing Results

The results obtained demonstrate some of the important system settings for gas detection. These results also demonstrate the difficulties encountered with the on-line processing methods.

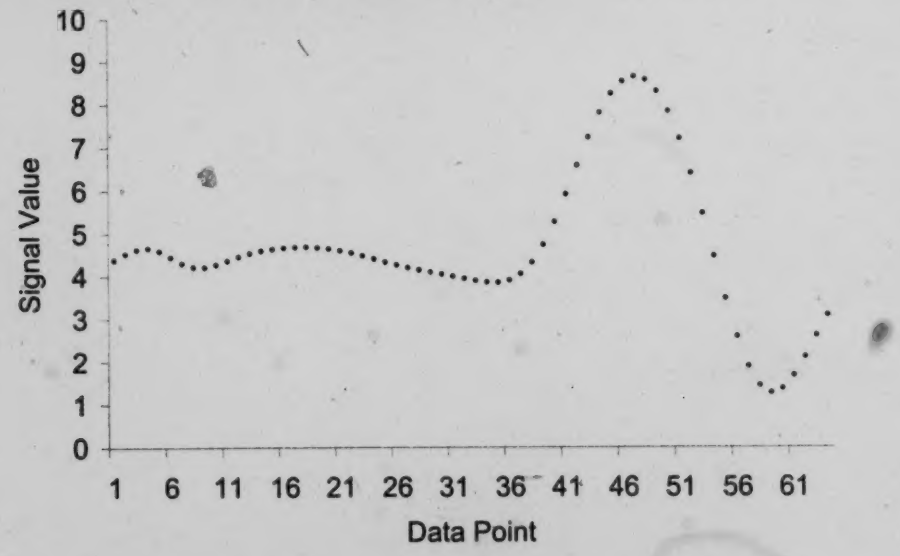

Figure 5.8: On-line Acquired Reference Signal Example

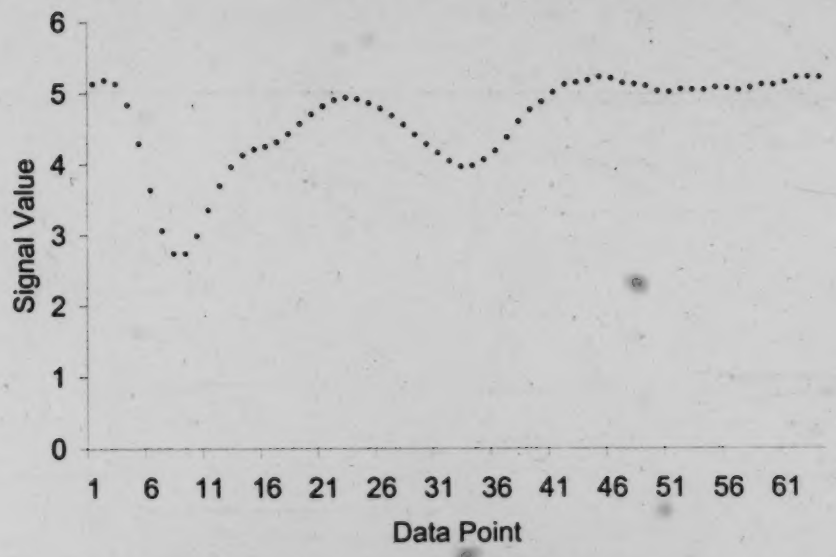

Figure 5.9: On-line Acquired Signal Example

Figures 5.8 and 5.9 show typical data obtained and used by the on-board processor for gas detection calculations. Signal size is given in the arbitrary units used by the computer. The amount of data taken during a signal sweep is limited to 64 data points. However, not all of these data points are included in the analysis because the first 14 data points are normally eliminated due to phase noise corruption.

The first test of the on-line processing algorithms involved placing the 8000 PPMM reference cell in the optical test base. Figure 5.10 shows the results of this test and proves that the instrument detects H_2S and is calibrated. It is easily noted that the perceived gas concentration falls periodically. This is related to the temperature of the laser diode wavering slightly, which causes the detected gas signal to move horizontally on the ramp scans. When this occurs, the stored reference signal does not move correspondingly, and therefore we see a fall of both the calculated gas concentration and the coefficient of linear correlation. By refreshing the reference waveform more often, the error in the calculated gas concentration is minimized since the stored reference waveform will match the test gas signal more precisely. However, we are left with a trade-off between the instrument accuracy and the amount of time between successive gas detection readings.

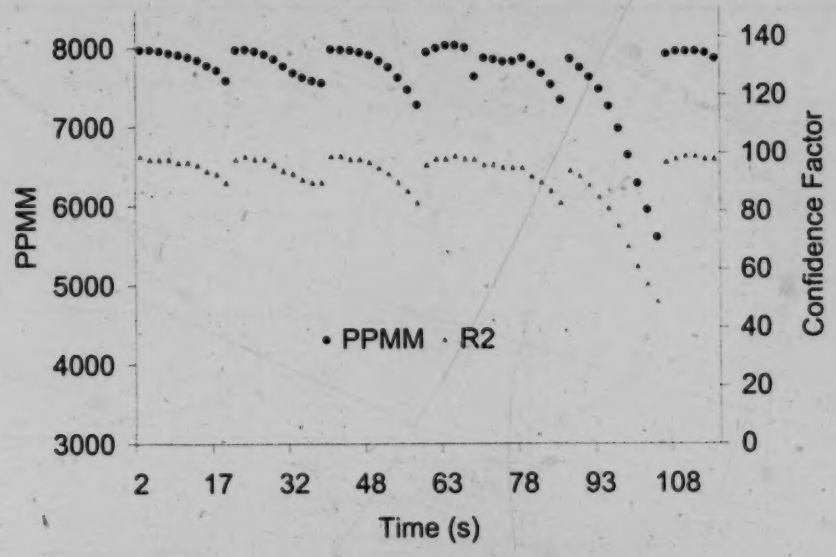

Figure 5.10: On-line Processing 8000 PPMM Gas Test

By refreshing the reference cell between each signal analysis, the results plotted in Figure 5.11 were obtained. By updating the reference waveform for every acquisition, we can estimate that the error in calculated gas concentration using the standard on-line signal processing is ~ 20 PPMM. The average gas concentration read by the instrument is 8025 PPMM when an 8000 PPMM cell was placed in the optical test bed. This small discrepancy is due to an error in the reference gas cell concentration used in the ratiometric gas calculations. The absolute average of the gas concentration can be set by changing the reference cell gas concentration used.

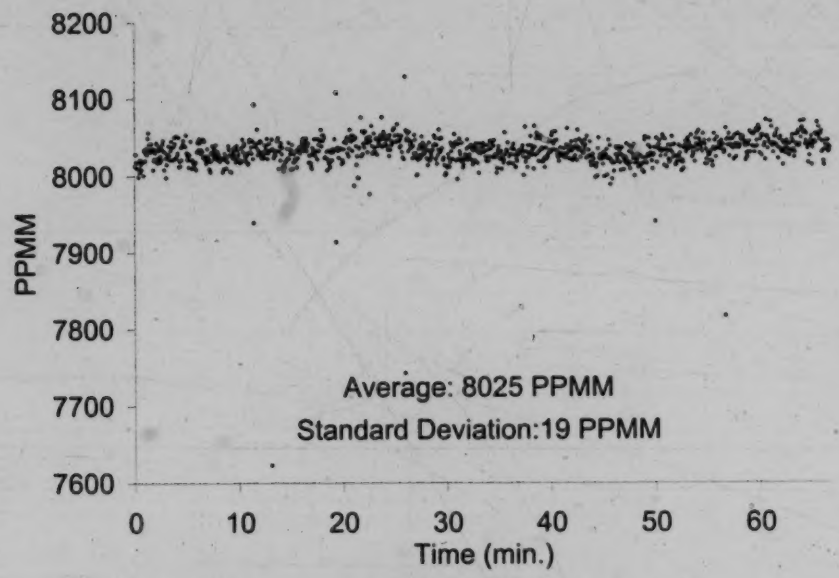

Figure 5.11: Stability of Gas Readings

The effect of the signal noise imprinted on the probe beam is shown in Figure 5.12. These results show the calculated gas reading obtained over a 35 m path. This figure shows that the imprinted noise, demonstrated in Figure 5.6, will cause erroneous readings which will vary depending on the form and position of the noise structure imprinted on the signal sweeps. It should be noted that this data is taken as an example. It should not be taken that the system will always give a false reading of ~ 37 PPMM. Experience with the system has shown instances that this background PPMM reading can float as high as 200 PPMM.

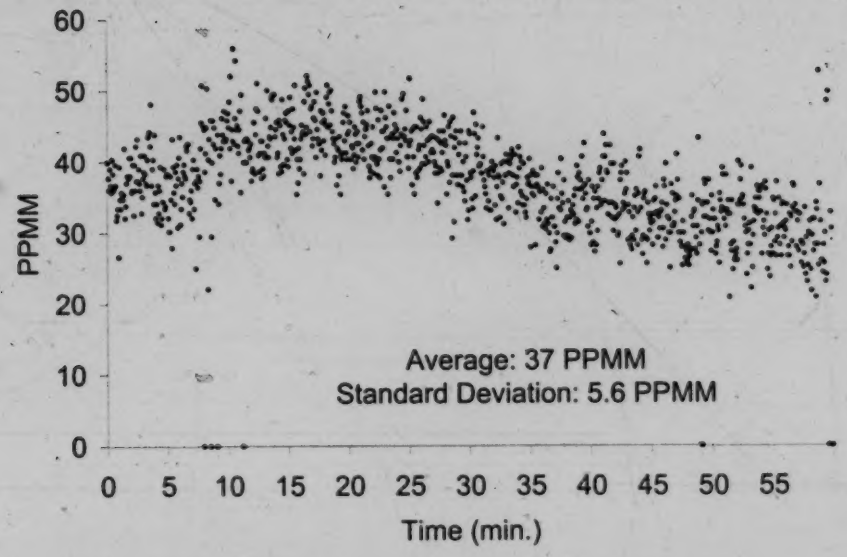

Figure 5.12: Standard On-line Processing Gas Detection Error

The existence of noise in the signal scans is unavoidable and leads to erroneous gas readings such as those given in Figure 5.12. However, it has already been pointed out that the imprinted noise can vary a great deal. §5.3.1 discusses the possibility that the ratiometric gas concentration calculation can yield a negative concentration if the signal waveform appears like the negative of the reference gas signal waveform. Thus, in a case where the imprinted noise roughly satisfies this criteria, the calculated gas concentration would be a negative number. The online processing computer cannot process negative gas concentration readings and therefore displays a zero concentration with a zero confidence factor when this occurs.

This case has been observed while using the standard processing mode. When this occurred, the computer provided a perceived gas concentration of zero, even though imprinted noise structure was plainly visible. It is therefore important to note that the problems associated with the imprinted noise are not restricted to causing higher calculated gas concentration readings. They can, in certain situations, reduce the perceived gas concentration below zero.

5.6.2 On-line Background Subtraction Results

Figure 5.13, demonstrates the usefulness of the on-line background subtraction routine. The first 40 calculated gas concentrations were taken without the use of background subtraction. The figure demonstrates that after background subtraction was applied, the gas concentration immediately fell to zero. Between the 38 minute mark and the 70 minute mark, we note that the perceived gas concentration rises for approximately 30 minutes. This is due to the acquired background no longer being representative of the scan waveform noise characteristics and thus the perceived gas concentration changes. Soon after, however, the gas concentration fell to zero and remained that way for several hours following. (These data are not included in the plot.)

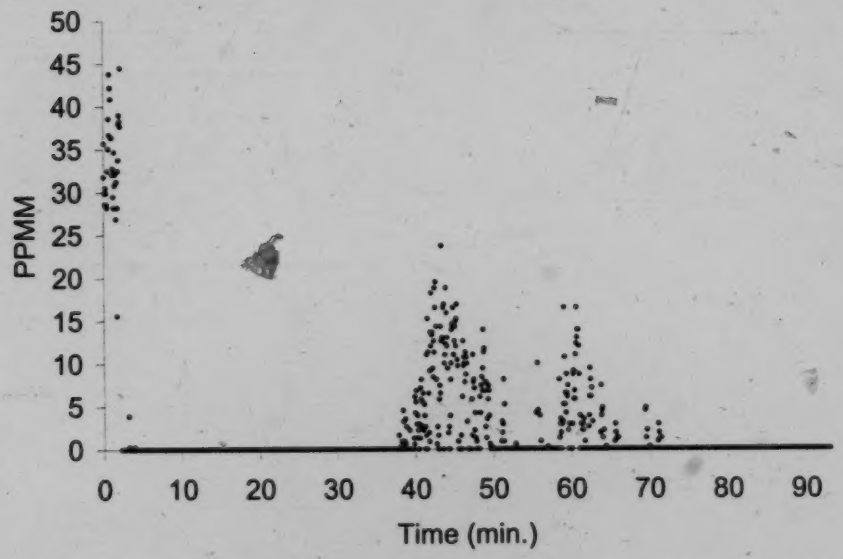

Figure 5.13: Online Background Subtraction Algorithm Testing

The fact that the perceived gas concentration never rose above zero after many hours of monitoring demonstrates a weakness in this noise processing method. To explain this weakness, we note that the background waveform acquired will have a characteristic gas concentration when it is analyzed using the ratiometric gas detection method. When we subtract a background waveform from the acquired signal we are effectively moving the perceived gas concentration level of

the instrument back to zero. Therefore, if the acquired background waveform has a larger gas concentration than the signal waveform, we might expect a negative calculated gas concentration. This is what occurred when the calculated gas concentration falling to zero for hours after the background waveform was acquired.

This highlights the importance of the stored background waveform in this processing method. While the unprocessed noisy scans cause the perceived gas concentration to sometimes float around an arbitrary concentration depending on the form of the imprinted noise. This method provides a way of eliminating the erroneous perceived gas concentration. However, in the on-line processing case, this can cripple the system by subtracting a waveform that causes the calculated gas concentration to dip below zero. The system would therefore then require a gas signal equal to or greater than the negative calculated gas concentration before the system would then perceive a gas presence, and even then the resultant gas concentration measurement would be lower than the actual concentration.

5.6.3 Standard Off-line Processing Results

The methods used to obtain the results outlined in this section are dependent on both a computer and an oscilloscope, and therefore should be considered experimental. While the basic principles and operating parameters would be roughly the same as described here, the sampling rate of the Analog to Digital conversion and the numerical precision used in the computations would likely need to be changed for ease in hardware implementation.

The Freedom16 computer board was not programmed such that it would accept commands from an outside source. As a result, the off-line computer is not able to control when the system checks the reference cell and therefore cannot update the reference waveform. The computer is also unable to query the onboard computer for the received light level of the reference and probe arms. Therefore, it is unable to properly calibrate the PPMM readings or even to tell whether the probe beams are blocked or. In order to properly evaluate the system sensitivity it was necessary to obtain sample light values for each arm and the reference waveform. By transferring the internal data array of the Freedom16 board, via the serial port, sample light values were obtained. The reference waveform

was acquired manually form the oscilloscope. Because these data could not be updated, extreme care was necessary during data acquisition to ensure that the operational parameters remained constant during the entire test.

Another result of the inability to communicate between the on-line and off-line computer, was that the amount of gain switching the used by the receiver board was inaccessible. The only method of obtaining the gain switching information was through a dump of the on-board computer data. Acquisition of these data arrays in real-time was not completed due to time constraints. As a result of this limitation, any signal that was large enough to require gain switching, i.e. test reference cells, would create an erroneous gas concentration reading.

All the data presented in this section assume the use of the averaging mode of the oscilloscope. The oscilloscope stored 256 averages of the signal and used a "revolving door" approach to updating the average, which is to say that the newest signals were always added to the stored 256 signals and the oldest signals were then thrown out. Using the fact that the waveform is acquired at 354 Hz, a quick calculation yields that every 723 mS the averaged waveform will be completely new. Therefore care was taken not to acquire the averaged waveform any quicker than this rate, as to avoid counting the signal scans more than once.

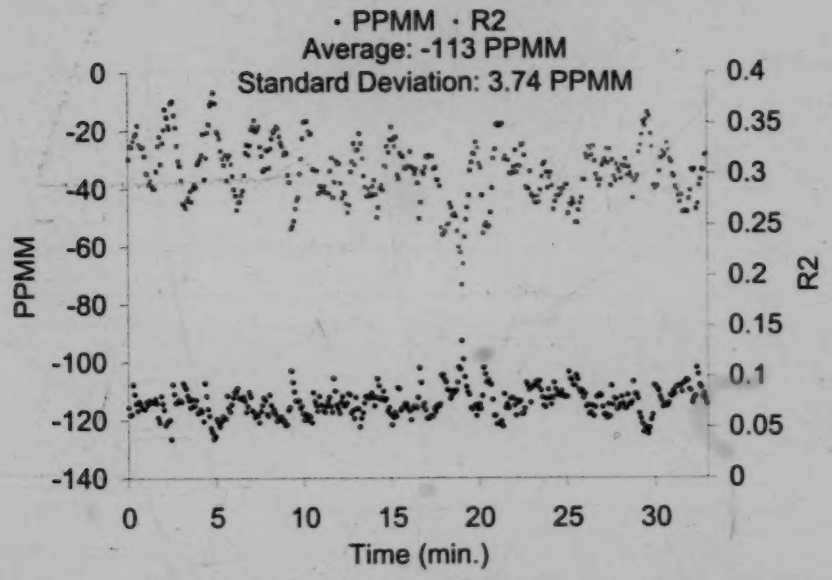

Figure 5.14: Raw Acquired Signal Calculated PPMM Readings

Figure 5.14 provides considerable insight into the problems that the imprinted noise causes in gas concentration calculations. We note that the average PPMM value is an unphysical negative gas concentration. This occurred because of background signal characteristics which are roughly the negative of the reference waveform. This possibility was discussed in §2.1.1. However, it is important to note the stability of the gas concentration reading. The standard deviation of the gas concentration reading is 3.74 PPMM, which is much better than the stability of the on-line processing results shown in Figure 5.11 This is due to a more relevant acquisition window and more samples being taken.

5.6.4 Off-line Background Subtraction Results

Off-line processing allowed the background subtraction method to be investigated further than was possible with the on-board computer algorithm. In order to determine the optimal method of background subtraction to eliminate the problems associated with imprinted noise, a large sample set was acquired. This sample set contained 1000 averaged scan waveforms with a 3 second delay between acquisitions. Thus the performance of the instrument is evaluated over ~ 50 minutes. Each scan was sampled at 1024 data points over a window defined by the edges of

the reference waveform. Figure 5.15 shows a comparison between an unprocessed waveform and one that has had a previous scan subtracted from it. A scaled down reference waveform is included to show the position of the gas signal.

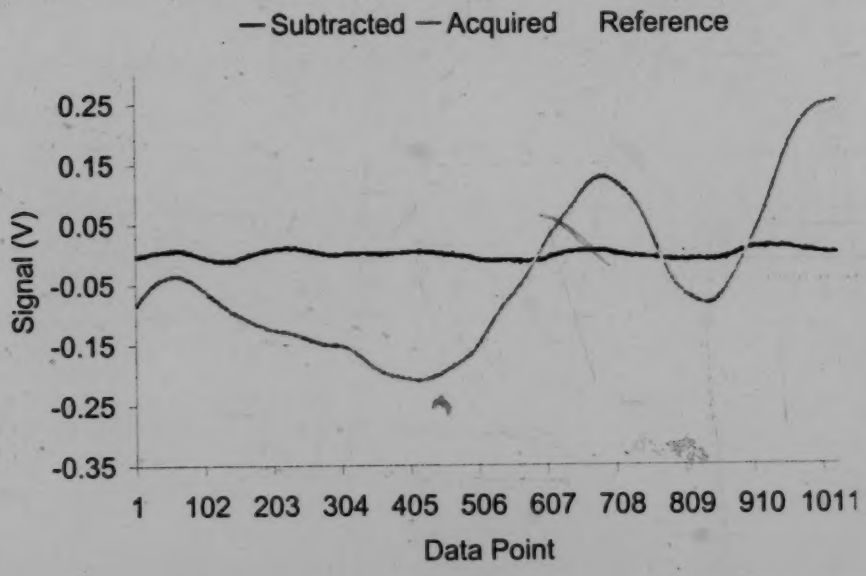

Figure 5.15: Background Subtraction Improvements on Signal Waveform

From this figure we can see that the subtracted waveform example effectively cancels out the acquired waveform. The small deviations that are left result from the difference between the background waveform used and the acquired waveform. Another point of interest is the relation of the acquired waveform to the reference gas signal. We note that a peak in the acquired array corresponds to the negative lobe of the reference array. This is precisely the situation which was outlined in §2.1.1. In fact, the PPMM reading of this acquired waveform is negative. By subtracting off a background array we expect the PPMM value to return to near zero.

For the purposes of testing the background subtraction algorithm, the confidence factor set point, *R*, was set to 1, the highest value it can have. This was done because during testing no gas was present in the optical path. Therefore, all the waveforms should be eligible background waveforms. The second parameter to be evaluated is the wait index. If the noise structure imprinted on the scan waveform varies in time, we

would expect that there would be an optimal choice of wait index to minimize the error in the perceived gas concentration. A sample set of 1500 waveforms (1 acquisition taken every 30 seconds) was built in order to monitor the effects of the wait index used. The background subtraction algorithm was then performed on the sample set for all possible wait indices. Figure 5.16 shows how the average gas concentration for the data set varies with respect to the wait index used. Calculated gas concentrations for the first *N* waveforms, where the wait index meant that no background waveform existed, were excluded.

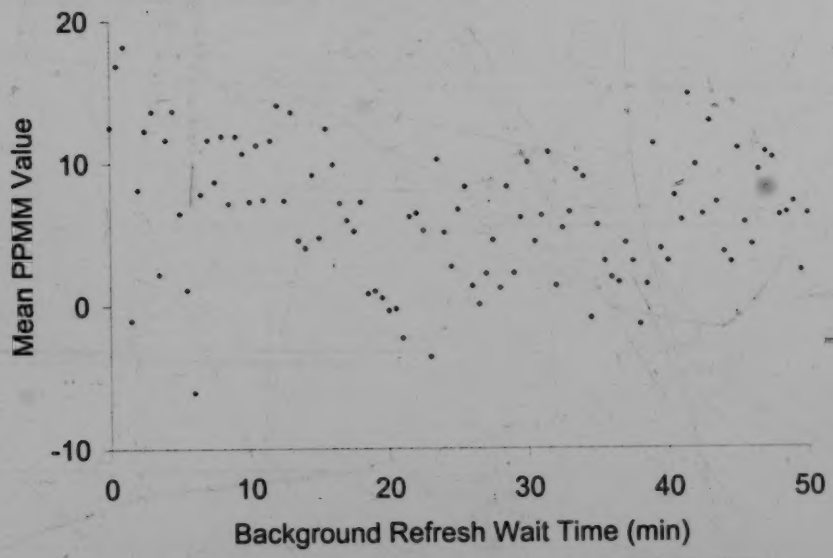

Figure 5.16: Wait Index Effects on a Sample Sets Average Gas Concentration

The results of this test show that there is no optimal wait index for intervals of less than 30 s. If the data set had been acquired with more temporal resolution, shorter wait indices could have been evaluated. However, it is unlikely that an engineered, multiple detection site system would be capable of updating the background waveform any quicker. It should be noted that the average gas concentration of all the possible wait indices is close to zero PPMM, which is encouraging.

Using an arbitrary wait index of 30 seconds, the following plot demonstrates the perceived gas concentration obtained over an hour of monitoring.

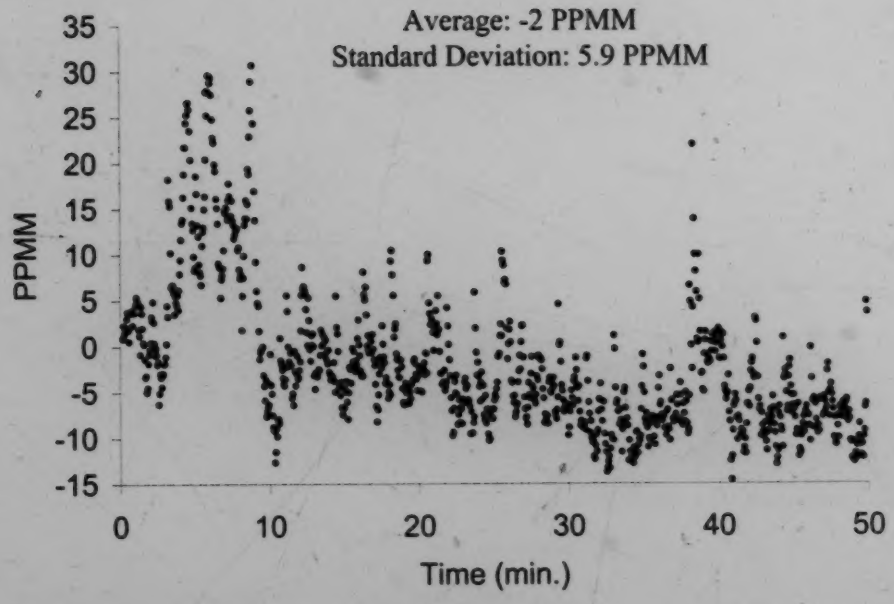

Figure 5.17: Background Subtracted Error in Calculated Gas Concentration

5.7 Minimum Sensitivity

A true test of the sensitivity of the instrument is impossible considering the current configuration and limitations imposed by the on-line computer. In order to obtain the minimum sensitivity of the instrument, accurate control of the transmitter board, analog switch and receiver would be necessary such that real time processing of the acquired signals would be possible. To perform this test, the off-line processing computer would need to be able to update both its L.V. and reference cell waveform, which it cannot presently do.

Even though a rigorous test of the system sensitivity is not possible, some general results about the sensitivity of the instrument can be stated. First, we can state that the instrument is likely not capable of detecting path gas concentrations of less than 20 PPMM. Even if the instrument is capable of detecting such low concentrations, the standard deviation of the results obtained in the previous sections raises doubts about the calibration stability of the gas concentration readings. With a

standard deviation of ~10 PPMM, we cannot not expect any accuracy in detection of gas levels below 20 PPMM.

However, it should be stated that the theoretical sensitivity of the instrument is much better than 20 PPMM. There are a great deal of possible improvements to be made to the signal and this will lead to further instrument signal stability and lower perceived gas concentrations. It is presumed that with further testing and the use of DSP software, the minimum detectable gas concentration could be lowered to the 1 PPMM regime.

5.8 Calibration Error

As discussed in §2.1.1, the ratiometric method of calculating the detected gas concentration uses several key data values to determine the perceived gas concentration. These values are the slope of the linear fit between the reference cell and the acquired waveform, the reference cell gas concentration, and the L.V. readings for both the reference cell and the acquired signal.

The error in the slope of the linear fit depends on the quality of the fit. This was normally measured via the coefficient of linear correlation. If the linear fit is of low quality, the error in slope will be high. Therefore, the error in calibration will be highest with low quality correlations and will decrease as the coefficient of linear correlation rises. The coefficient of linear correlation is lowest when no gas is present and therefore we must conclude that this is when the error in perceived gas concentration will be the highest.

The error in the reference cell gas concentration is arbitrary. Filling small reference cells with a defined concentration is a difficult endeavor, especially with toxic gases like H_2S. It is therefore assumed that the reference cell gas concentration has an error of 10%.

Error in L.V. readings depends on the processing methods used. For the on-line processing case, the error will be small sine the value used is updated regularly. Over 1000 readings taken using on-line processing, the error in L.V. was 0.2 %. However, the error in L.V. readings is much higher for the off-line processing case as the L.V.

readings were acquired once at the beginning of the analysis and never updated for the entire data acquisition run.

Using standard propagation of uncertainties [55], we can determine the error in the perceived gas concentration. This calculation assumes no error in the acquired signal waveforms. This is obviously not the case. However, as a first measure of accuracy, this calculation provides a minimal estimation of the perceived gas concentration error. Because the error in the linear fit slope varies a great deal depending on the form of the acquired waveforms, we will use an arbitrary error of 10 %. Using this assumption, we obtain an error in the perceived gas concentration of approximately 15 %. However, for the data plotted in Figure 5.17, the average error in slope is greater than 100% ! This shows how unreliable the perceived gas concentration is when no gas is present. It is true that the slope is obtained through a least squares approximation and should be a good guess of the gas concentration, but the error in slope is a difficulty which must be considered when no gas is present.

This preliminary error analysis illustrates the most important aspect of using this instrument for gas detection. When there is no gas present in the optical probe beam path, the perceived gas concentration is extremely unreliable. When the gas concentration increases, the error in the perceived concentration will fall making the estimation of average gas concentration more trustworthy. In other words, when the system is used to detect extremely low gas concentrations, ie < 50 PPMM, the instrument will only indicate that some gas is present. The absolute amount is unreliable.

6. Conclusions

This project shows that by using TDLS, it is possible to detect gases at remote locations. While the system was tailored to the detection of H_2S, the methods developed would apply equally well to any gas with an absorption profile in the 1.3 μm to 1.7 μm wavelength region. Therefore, the methods outlined in this thesis provide the necessary framework for the deployment of a fiber optic network capable of detecting several gases in many locations. While much more development is needed, the fundamental issues in implementation have been investigated.

The most important research completed is the evaluation of the use fiber optics in a TDLS gas detection system. While fundamental research into fiber optics technology has shown little evidence to question the use of fiber, extensive testing and experience has demonstrated some important difficulties that arise from its use. One of the problems encountered in this test project was the presence of imprinted noise on the signal scans. Other researches have noted that fiber backreflections cause this etalon noise, which limits the sensitivity of the instrument. However, it is possible to compensate for these problems using background subtraction techniques.

One of the accomplishments of this project involves the successful use of fiber optic splitters. These splitters do not induce noise in the TDLS process, are inexpensive, and allow the division of light onto several detection paths. While the splitters used in this project were 1X2 and 1X4, the light division methods used in splitters do not effect the probe light and therefore other splitter types and splitting ratios can be used.

The use of a MultiMode fiber optic link to return the signal from the remote heads to the central system was also a success. This link provided the bandwidth required and insulates the signal from any unwanted electromagnetic interference. Other methods of returning the signal to central receiver and processing are possible since all that is required is a link with a minimum of 25 MHz of bandwidth. However, the use of a fiber optic link provides both economy and guarantees clean signal transport.

In the domain of signal processing, background subtraction has shown significant promise. As the imprinted noise structure is stable in the short term it seems entirely feasible to subtract this "constant" to minimize erroneous gas concentrations. The analysis and testing performed in this project provide a good basis from which the algorithm could be built.

However, it is important that the background subtraction routine not subtract any real gas signal. The use of the confidence factor, *R*, is one possible way of assuring that the background waveform used does not contain gas like signals. The use of the wait index provides a time delay for the background waveform update, but Figure 5.16 does not suggest an optimal wait time. Further research into the response time of the instrument would provide valuable insights for the choice of wait index, *N*.

This leads us to the fundamental limitation of the testing apparatus built during this project. The inclusion of the Boreal Laser GasFinder into the heart of the system lead to many signal processing difficulties. A system developed for further testing should rely on the use of a PC to provide maximum versatility and system control. Reliable testing demands that all pertinent system parameters be controlled accurately. The temperature, laser diode injection current, receiver gain, switch control, and L.V. calibration were all controlled by the on-line computer while the off-line computer acquired the signals and processed them. This has led to the possibility of erroneous reference cell signals being passed to the off-line computer when it does not expect them. This has also led to the off-line processing inability to calibrate the perceived gas concentration with detected L.V..

While it would be possible to implement the processing techniques evaluated in this thesis directly into a working developmental project, further off-line integration would yield extremely valuable diagnostic insights into the operation of on-site gas detectors. That is, an off-line platform for complete control of all essential system parameters would yield not only further development ease, but also a method of diagnosing any failures from which an on-line computer system is suffering from. The use of LabVIEW allows for modularity in integrating processes and also for ease in system parameter monitoring.

The quality of the laser diode packaging has come under considerable scrutiny considering the amount of noise imprinted on the probe beam. However, the laser package is valued at over $7000 and therefore purchasing other diodes for comparison was not an option. Better isolation, ~ 60 dB, and more efficient fiber coupling, ~80%, are both possible improvements that could be made. These are options to be considered in the next generation of fiber optic GasFinder technology.

The use of a poor quality retroreflector may also degrade system sensitivity. It was observed during the research for an all-optical remote head that a low quality retroreflector induces considerable phase distortion between the 6 possible reflection paths. Therefore the reflected beams will interfere at the focus of the collection optic and cause a variation in the intensity of the received signal. Turbulence will induce phase distortions on a time scale that could be comparable to the ramp sweep, and hence inducing another type of turbulence dependent system noise. However, because of the amount of averaging that is performed on the signal during its processing it is unlikely that this interference noise effect will be constant over the averaging period and will therefore be transparent. Further exploration of turbulence effects on TDLS gas detection methods is required.

References

1. Alberta Labour Occupational Health & Safety Bulletin: Medical Guideline, Guideline on the Treatment of Hydrogen Sulfide Poisoning, MSB-05, August 1994

2. This information is readily available on the internet.

3. G. C. Bjorklund, "Frequency-modulation spectroscopy: a new method for measuring weak absorptions and dispersions", Optics Letters, Vol. 5, pp.15-17, 1980

4. W. Lenth, "High Frequency Heterodyne Spectroscopy with Current-Modulated Diode Lasers", IEEE J. Quantum Electronics, Vol. QE-20, No. 9, pp. 1045-1050, 1984

5. K. Petermann, Laser Diode Modulation and Noise, Kluwer Academic Publishers, Tokyo, pp. 119-144, 1988

6. J. A. Silver, "Frequency-modulation spectroscopy for trace species detection: theory and comparison among experimental methods", Applied Optics, Vol. 31, No. 6, pp. 707-717, 1992

7. J. M. Supplee, E. A. Whittaker and W. Lenth, "Theoretical description of frequency modulation and wavelength modulation spectroscopy", Applied Optics, Vol. 33, No. 27, pp. 6294-6302, 1994

8. D. E. Cooper and R. E. Warren, " Two-tone optical heterodyne spectroscopy with diode lasers: theory of line shapes and experimental results", J. Opt. Soc. Am. B, Vol. 4, No. 4, pp. 470-480, April 1987

9. G. R. Janik, C. B. Carlisle and T. F. Gallagher, "Two-tone frequency-modulation spectroscopy", J. Opt. Soc. Am. B, Vol. 3, No. 8, pp. 1070-1074, August 1986

10. J. Reid and D. Labrie, "Second-Harmonic Detection with Tunable Diode Lasers – Comparison of Experiment and Theory", Appl. Phys. B, Vol. 26, pp. 203-210, 1981

11. R. Arndt, "Analytical Line Shapes for Lorentzian Signals Broadened by Modulation", J. Appl. Phys., Vol. 36, No. 8, pp. 2522-2524, 1965

12. M. Gehrtz, W. Lenth, A. T. Young, and H. S. Johnston, "High frequency-modulation spectroscopy with a lead-salt diode laser", Opt. Lett., 11, pp. 132-134, 1986

13. J. A. Silver and A. C. Stanton, "Two-tone optical heterodyne spectroscopy using buried double heterostructure lead-salt diode lasers", Appl. Opt., Vol. 27, pp. 4438-4444, 1988

14. G. J. Meslener, "Chromatic Dispersion Induced Distortion of Modulated Monochromatic Light Employing Direct Detection", IEEE J. Quantum Electronics, Vol. QE-20, No. 10, pp. 1208-1216, October 1984

15. G. B. Arfken and H. J. Weber, Mathematical Methods for Physicists, Academic Press, Toronto, p. 639, 1995

16. G. C. Bjorklund and M. D. Levenson, "Frequency Modulation Spectroscopy", Appl. Phys. B., Vol. 32, pp. 145-152, 1983

17. D. S. Bomse, A. C. Stanton and J. A. Silver, "Frequency Modulation and wavelength modulation spectroscopies: comparison of experimental methods using lead-salt diode laser", Appl. Optics, Vol. 31, No. 6, pp. 718-731, 1992

18. A. M. Ballangrud, Diode laser spectroscopy for gas monitoring of environmental pollution and for industrial process and emission control, University of Oslo Thesis, Oslo, 1993

19. L. Lechuga-Fossat, J.-M. Flaud, and C. Camy-Peyret, "The H2S spectrum in the 1.6 μm region", Molecular Physics, Vol. 61, No. 1, pp. 23-32, 1987

20. V. Weldon, J. O'Gordon, P. Phelan, and T. Tanbun-Ek, "Gas sensing with λ=1.57 μm distributed feedback laser diodes using overtone and combination band absorption", Optical Engineering, Vol. 33, No. 12, pp. 3867-3870, December 1994

21. E. Hecht, Optics, Addison-Wesley Publishing Co., Don Mills, Ontario, pp. 92-99, 1974

22. E. Hecht, Optics, Addison-Wesley Publishing Co., Don Mills, Ontario, pp. 367, 1974

23. G. Stewart, A. Mecaglia, W. Philp and W. Jin, "Interferometric Signals in Fiber Optic Methane Sensors with Wavelength Modulation of the DFB Laser Source", J. Lightwave Technology, Vol. 16, No. 1, pp. 43-53, January 1993

24. W. Jin, Y. Z. Xu, M. S. Demokan and G. Stewart, "Investigation of intereferometric noise in fiber-optic gas sensors with use of wavelength modulation spectroscopy", Applied Optics, Vol. 36, No. 28, pp. 7239-7246, October 1997

25. H. C. Sun, and E. A. Whittaker, "Novel etalon fringe rejection technique for laser absorption spectroscopy", Applied Optics, Vol. 31, No. 24, pp. 4998-5002, August 1992

26. C. R. Webster, "Brewster-plate spoiler: a novel method for reducing the amplitude of interference fringes that limit tunable-laser absorption sensitivities", J. Opt. Soc. Am. B, Vol. 2, No. 9, pp. 1464-1470, September 1985

27. X. Zhu, and D. T. Cassidy, "Electronic subtractor for trace-gas detection with InGaAsP diode lasers", Applied Optics, Vol. 34, No. 36, pp. 8303-8308, December 1995

28. D. A. Glenar, D. E. Jennings, and S. Nadler, "Electrooptic modulation methods for high sensitivity tunable diode laser spectroscopy", Applied Optics, Vol. 29, No. 15, pp. 2282-2288, May 1990

29. H. Riris, C. B. Carlisle, L.W. Carr, D. E. Cooper, R. U. Martinelli, and R. J. Menna, "Design of an open path near-infrared diode laser sensor: application to oxygen, water, and carbon dioxide vapor detection", Applied Optics, Vol. 33, No. 30, pp. 7059-7066, October 1994

30. H. Riris, C. B. Carlisle, R. E. Warren, and D. E. Cooper, "Signal-to-noise ratio enhancement in frequency-modulation spectrometers by digital signal processing", Optics Letters, Vol. 19, No. 2, pp. 144-146, January 1994

31. C. Y. Kuo, "Fundamental Nonlinear Distortions in Analog Links with Fiber Amplifiers", J. Lightwave Technology, Vol. 11, No. 1, pp. 7-15, January 1993

32. Marconi Materials Technology Ltd., LD6204 Advance Product Information, Marconi Electronic Systems

33. Wavelength Electronics Inc., LDD P series Specification Sheet, Wavelength Electronics Inc., 51 Evergreen Dr. Suite B, Bozeman, MT, 59715, USA

34. Marlow Industries Inc. tH3 Bead Thermistor 2228-05, 10451 Vista Park Road, Dallas, Texas, USA

35. Hytek Microsystems, HY5610 TEC Controller – Subminiature Controller for Thermoelectric Coolers, Hytek Microsystems, 400 Hot Springs Rd., Carson City NV, USA

36. Technical Staff of CSELT, Fiber Optic Communications Handbook, TAB Professional and Reference Books, Blue Ridge Summit, PA, 1981

37. J. A. Arnaud, Beam and Fiber Optics, Academic Press, New York, 1976

38. W. van Etten, and J. van der Plaats, Fundamentals of Optical Fiber Communications, Prentice Hall, New York, 1988

39. D. G. Baker, Fiber Optic Design and Applications, Reston Publishing Company, Virginia, 1985

40. B. E. Briley, Introduction to Fiber Optics System Design, North-Holland, New York, 1988

41. W. B. Jones, Introduction to Optical Fiber Communications Systems, Holt, Rinehart and Winston Inc, Montreal, pp. 99-106, 1988

42. R. W. Gilsdorf, and J. C. Palais, "Single-mode fiber coupling efficiency with graded-index rod lenses", Applied Optics, Vol. 33, No. 16, pp. 3440-3445, June 1994

43. F. C. Allard, Fiber Optics Handbook for Engineers and Scientist, McGraw-Hill Publishing Co., Toronto, pp. 3.13-3.14, 1990

44. C. DeCusatis, E. Maass, D. Clement, and R. Lasky, Handbook of Fiber Optic Data Communication, Academic Press, Toronto, 1998

45. B. E. A. Saleh, and M. C. Teich, Fundamentals of Photonics, Wiley-Interscience Publications, New York, pp. 86, 1991

46. F. C. Allard, Fiber Optics Handbook for Engineers and Scientist, McGraw-Hill Publishing Co., Toronto, pp. 3.4-3.4.2, 1990

47. O. M. Sezerman, Tilt adjustable optical fibre connectors, US Patents #4753510 & 4889406, Canadian Patents #1258786 & 1325112

48. EG&G Canada Ltd. Optoelectronics Division, Large Area InGaAs Photodiodes Datasheet, 22001 Dumberry Road, Vaudreuil, Quebec, Canada

49. Analog Modules Inc., Model 111 Specification Sheet, 126 Baywood Ave, Longwood Florida, USA

50. R. L. Fante, "Electromagnetic Beam Propagation in Turbulent Media", Proceedings of the IEEE, Vol. 63, No. 12, pp. 1669-1692, December 1975

51. V. E. Zuev, Laser Beams in the Atmosphere, Consultants Bureau, New York, p. 242, 1983

52. Fiber Options Inc., Series 175B Operating Instructions Document #201753.2, 80 Orville Drive, Suite 102, Bohemia, New York, USA

53. Intec Automation Inc., Freedom 16 v2.1 Users Manual, 2751 Arbutus Road, Victoria BC, Canada

54. Boreal Laser Inc., GasFinder 2.0, Portable System, Operation Manual, #13 – 51127 RR 255, Spruce Grove AB, Canada

55. J. R. Taylor, An Introduction to Error Analysis, University Science Books, USA, pp. 153-162, 1982

Appendix A

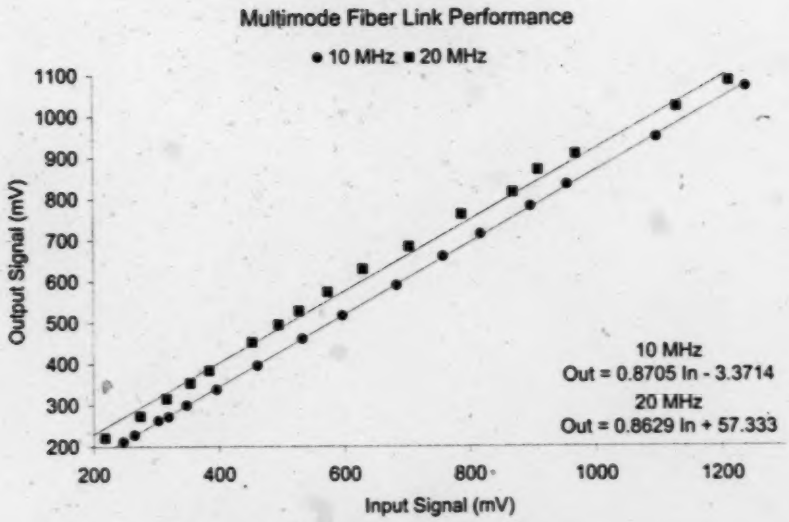

Figure A.1: Operating Characteristics of the Fiber Options 175B Video Transmission Link

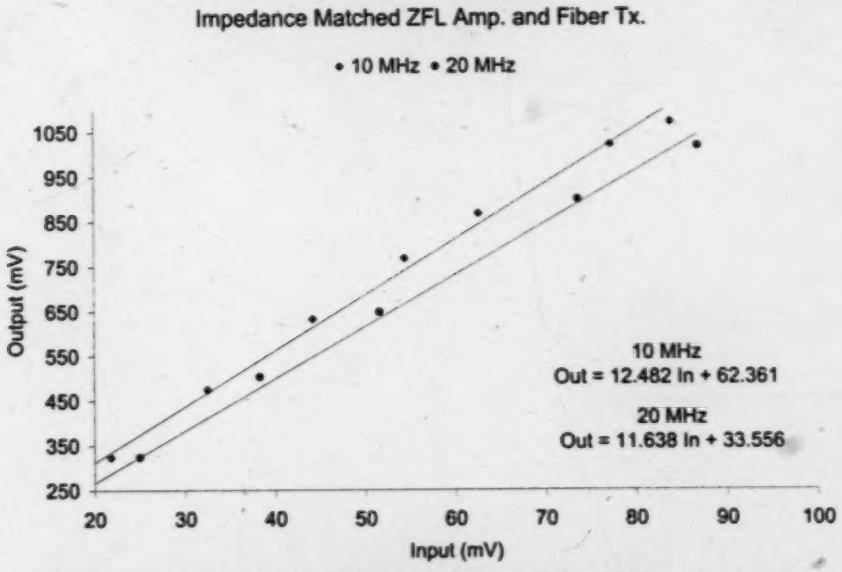

Figure A.2: Operating Characteristics of the Link with the ZFL Amp. Before the Transmitter Input

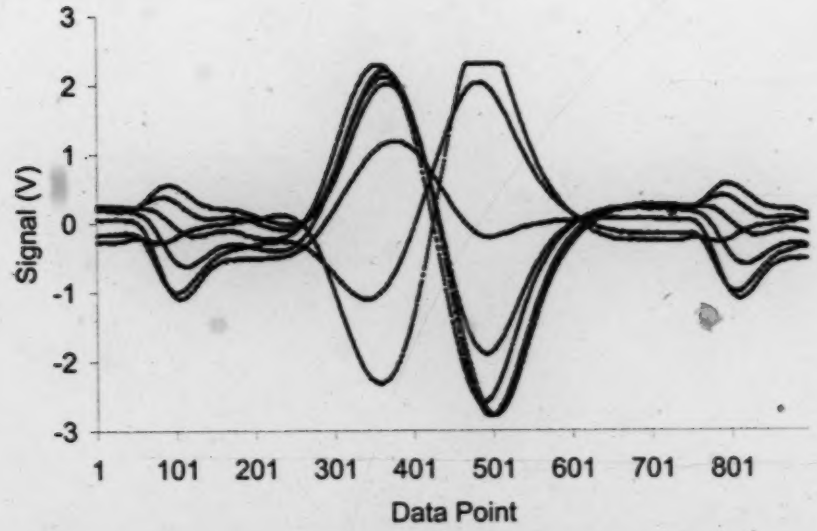

Figure A.3: Effect of an inaccurate Phase Shifter setting on the Reference waveform. Data taken every 5 complete turns of the shifter.

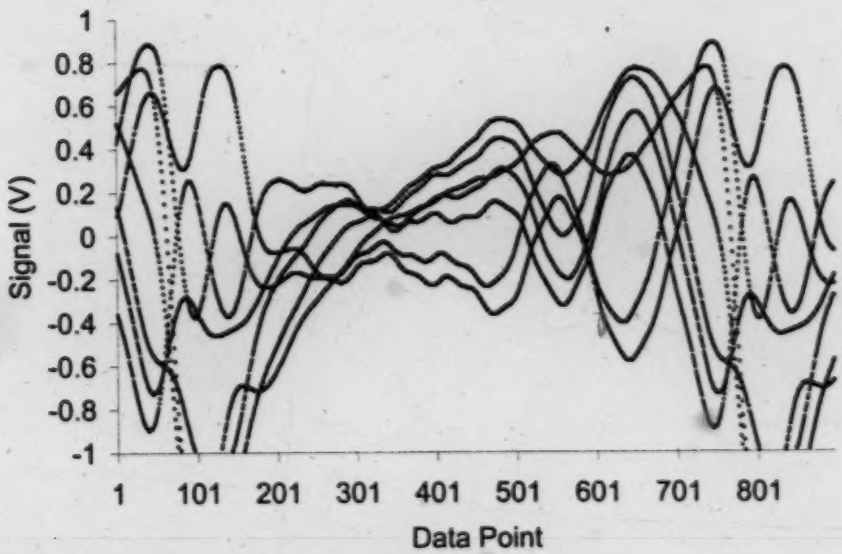

Figure A.4: Demonstration of the range of possible signal waveforms for all possible phase shifter settings.

Appendix B

Mathematica Programs

Definitions used in Mathematica Programs:

```
Speed of light
c = 3 10^8;
Operating Wavelength
lambda = 1.578 10^(-6);
Optical Frequency
w0 := 2 π c / lambda;
LineWidth - HWHM
delw = 0.175 c 100;
Line Strength - cm / mol
S = 1.3 10^(-20);
Modulation Frequency
wm = 2 * π * 10 * 10^6;
Pressure in atmospheres
P = 1;
Loschmidts Number - # Molecules / cm^3 / atm
NL = 2.479 * 10^19;
```

FMS Theoretical Functions:

```
Clear[alpha, r1, r3, rl, z];
g[w_] := delw^2 / ((w - w0)^2 + delw^2);
alpha[w_] := S * g[w] * NL * P * L;
r1[l_] := -m / (2 I) Exp[-I psi] BesselJ[l + 1, beta];
r3[l_] := m / (2 I) Exp[I psi] BesselJ[l - 1, beta];
rl[l_] := r1[l] + BesselJ[l, beta] + r3[l];
shift[w_] := -FiberDist * (2 π c / w)^2 / (4 π c) *
    Disp * wm^2;
```

Program used to calculate background for FMS:

```
filename1 = "E:/MathData/BackGroundSignal.txt";
Steps = OpenWrite[filename1, FormatType→ FortranForm];
Write[Steps, First Harmonic BackGround];
For[s = -500, s < 500, Write[Steps, s, q, w0 + (s * 2 * wm), q,
    Sum[(Re[rl[i] * rl[i - 1]]), {i, -110, 110}]], s++];
Write[Steps, Second Harmonic BackGround];
For[s = -500, s < 500, Write[Steps, s, q, w0 + (s * 2 * wm), q,
    Sum[(Re[rl[i] * rl[i - 1]]), {i, -110, 110}]], s++];
Close[filename1];
```

Example program for FMS Signal calculations:

```
FirstHarm = OpenWrite[filename2, FormatType → FortranForm];
Write[FirstHarm, First Harmonic Signal - First Num =
   For index - Second Num = Scan Frekuency - Third Num = Data];
For[s = -500, s < 500, Write[FirstHarm, s, q, (w0 + (s * 2 * wm)),
   q,
    Sum_{i=-110}^{110} (Re[rl[i] * rl[i - 1] *
        Exp[-0.5 * alpha[(w0 + (s * 2 * wm)) + i * wm] -
          0.5 * alpha[(w0 + (s * 2 * wm)) + (i - 1) * wm]]])], s++];
Close[filename2];
SecondHarm = OpenWrite[filename3, FormatType → FortranForm];
Write[SecondHarm, Second Harmonic Signal - First Num =
   For index - Second Num = Scan Frekuency - Third Num = Data];
For[s = -500, s < 500, Write[SecondHarm, s, q, (w0 + (s * 2 * wm)),
   q,
    Sum_{i=-110}^{110} (Re[rl[i] * rl[i - 2] *
        Exp[-0.5 * alpha[(w0 + (s * 2 * wm)) + i * wm] -
          0.5 * alpha[(w0 + (s * 2 * wm)) + (i - 2) * wm]]])], s++];
Close[filename3];
```

Example program to calculate etalon fringes:

```
etalondist = 0.010; reflect = 10^(-3);
delay = 2 * etalondist * 1.456 / c;
etalon1 = OpenWrite[filename8, FormatType → FortranForm];
Write[etalon1, First Harmonic 10 mm Etalon Signal with
   reflectis 0.001 ];
For[s = -500, s < 500,
  Write[etalon1, s, q, (w0 + (s * 2 * wm)), q,
    Sum_{i=-110}^{110} (Re[rl[i] * rl[i - 1]
        (1 + reflect * Exp[i * ((w0 + (s * 2 * wm)) + i * wm) *
             delay])
        (1 + reflect * Exp[-i * ((w0 + (s * 2 * wm)) + (i - 1)) *
             delay]))], s++];
```